Ö. DÜLGAR

A ROBUST ALTITUDE CONTROL APPROACH FOR SEA SKIMMING MISSILES

ÖZGÜN DÜLGAR

JANUARY 2018

METU 2018

A ROBUST ALTITUDE CONTROL APPROACH FOR SEA SKIMMING MISSILES

A THESIS SUBMITTED TO
THE GRADUATE SCHOOL OF NATURAL AND APPLIED SCIENCES
OF
MIDDLE EAST TECHNICAL UNIVERSITY

BY

ÖZGÜN DÜLGAR

IN PARTIAL FULFILLMENT OF THE REQUIREMENTS
FOR
THE DEGREE OF MASTER OF SCIENCE
IN
AEROSPACE ENGINEERING

JANUARY 2018

Approval of the thesis:

A ROBUST ALTITUDE CONTROL APPROACH FOR SEA SKIMMING MISSILES

submitted by **ÖZGÜN DÜLGAR** in partial fulfillment of the requirements for the degree of **Master of Science in Aerospace Engineering Department, Middle East Technical University** by,

Prof. Dr. Gülbin Dural Ünver _____
Dean, Graduate School of **Natural and Applied Sciences**

Prof. Dr. Ozan Tekinalp _____
Head of Department, **Aerospace Engineering**

Asst. Prof. Dr. Ali Türker Kutay _____
Supervisor, **Aerospace Engineering Dept., METU**

Examining Committee Members

Prof. Dr. Ozan Tekinalp _____
Aerospace Engineering Department, METU

Asst. Prof. Dr. Ali Türker Kutay _____
Aerospace Engineering Department, METU

Assoc. Prof. Dr. İlkay Yavrucuk _____
Aerospace Engineering Department, METU

Prof. Dr. M. Kemal Leblebicioğlu _____
Electrical and Electronics Engineering Department, METU

Asst. Prof. Dr. Yakup Özkazanç _____
Electrical and Electronics Engineering Department,
Hacettepe University

Date: _____

I hereby declare that all information in this document has been obtained and presented in accordance with academic rules and ethical conduct. I also declare that, as required by these rules and conduct, I have fully cited and referenced all material and results that are not original to this work.

Name, Last Name **:** ÖZGÜN DÜLGAR

Signature **:**

ABSTRACT

A ROBUST ALTITUDE CONTROL APPROACH FOR SEA SKIMMING MISSILES

Dülgar, Özgün
M.S., Department of Aerospace Engineering
Supervisor: Assist. Prof. Dr. Ali Türker Kutay

January 2018, 90 pages

A sea skimming missile is needed to be flown above mean sea level as low as it can, in order to decrease detectability; so that, survivability of the missile against counter attacks of the target ships is maximized. On the other hand, flying at very low altitude is a tough task under disturbances due to sea waves and measurement errors of various sensors used in height control loop. Thus, a robust altitude control system design is one of the main challenges among the other control algorithms for a sea skimming missile. In this study, Kalman filter based altitude control method is proposed and compared with the existing designs in literature. Moreover, determination of the optimal flight altitude is performed by estimating the instantaneous sea condition by Kalman filter. Simulation results for widely varied scenarios, in which different sensor errors, severe sea conditions, and limited computing power are taken into account, are shared. Results show that the proposed Kalman filter based altitude control application has satisfactory performance against many real world issues.

Keywords: Sea Skimming Guidance, Robust Height Control

ÖZ

SU SATHINA YAKIN UÇAN FÜZELER İÇİN GÜRBÜZ İRTİFA KONTROLÜ YAKLAŞIMI

Dülgar, Özgün
Yüksek Lisans, Havacılık ve Uzay Mühendisliği Bölümü
Tez Yöneticisi: Yrd. Doç. Dr. Ali Türker Kutay

Ocak 2018, 90 sayfa

Su sathına yakın uçuş yapan bir füze, fark edilebilirliğini düşürerek hedef geminin karşı saldırılarına karşı kendi bekasını artırabilmek için, ortalama deniz seviyesine göre olabildiğince düşük irtifada uçmalıdır. Diğer taraftan çok düşük irtifada seyretmek, irtifa kontrolü döngüsünde kullanılan çeşitli sensörlere ait pek çok hata ve deniz yüzeyindeki dalgaların yarattığı bozucu etkiler sebebiyle, oldukça zorlu bir görevdir. Bu yüzden, su sathına yakın uçan füzeler için, gürbüz bir irtifa kontrolü sisteminin tasarımı füze üzerindeki diğer kontrol algoritmalarının arasında en önemlilerinden birisidir. Bu çalışmada, Kalman filtresi tabanlı irtifa kontrol sistemi sunulmakta ve literatürde yer alan tasarımlar ile kıyaslanmaktadır. Bunun yanı sıra, anlık deniz koşulları kestirilerek, optimum uçuş yüksekliği de Kalman filtresi tarafından belirlenmiştir. Farklı sensör hataları, kötü deniz durumu, ve kısıtlı bilgisayar gücü gibi etkenlerin hesaba katıldığı pek çok farklı senaryo için benzetim sonuçları paylaşılmıştır. Sonuçlara göre, önerilen yöntem olan Kalman filtresi tabanlı irtifa kontrolcüsü pek çok gerçek dünya problemlerine karşı tatmin edici performans göstermektedir.

Anahtar Kelimeler: Su Sathına Yakın Uçuş Güdümü, Gürbüz İrtifa Kontrolü

to my father

ACKNOWLEDGMENTS

I would like to express the deepest appreciation to my supervisor Asst. Prof. Dr. Ali Türker Kutay for his patience, guidance and deep interest throughout the thesis study. Without his enthusiasm and support, this study would not have been possible. I also wish to express my sincere thanks to my committee members for their invaluable contribution and comments on this study.

I would like to thank my colleague in Roketsan Rüştü Berk Gezer for sharing his time, energy and knowledge whenever I needed. I would also like to thank Gökhan Tüşün, Koray Savaş Erer and Alper Kahvecioğlu for their invaluable support; they always helped me with useful discussions.

Above all, I would like to thank my sister Özden and my mother Emine for their endless love and unconditional support throughout my life. They have always faith on me.

Last but not the least important, I owe more than thanks to my dearest wife Pınar for her patience and love.

TABLE OF CONTENTS

LIST OF TABLES

TABLES

LIST OF FIGURES

FIGURES

LIST OF ABBREVIATIONS

CAS	Control Actuator System
CDF	Cumulative Distribution Function
CIWS	Closed In Weapon Systems
EKF	Extended Kalman Filter
ESO	Extended State Observer
FFT	Fast Fourier Transform
GPS	Global Positioning System
IMU	Inertial Measurement Unit
INS	Inertial Navigation System
KF	Kalman Filter
LQG	Linear Quadratic Gaussian
LQR	Linear Quadratic Regulator
LTI	Linear Time Invariant
PDF	Probability Density Function
RA	Radar Altimeter
RMS	Root Mean Square

CHAPTER 1

INTRODUCTION

Anti-ship missiles are guided missiles which have long being used in warfare on the sea against ships. They are able to be launched from several platforms, such as warships, submarines, aircrafts, and ground stations on coasts. Targets of these missiles are generally armed naval ships like frigates, destroyers, aircraft carriers and corvettes. Obviously, these battleships are equipped with very effective defense systems against any kind of attack, especially against air attacks. Almost all modern battleships are equipped with some kind of defense systems, the ones being used against air attacks, are named as closed in weapons system, or shortly CIWS. Several kinds of CIWS exist and being used in modern warships, examples of most of them and far-reaching information about how they work can be found in [1]. Another study [2], involves conceptual analysis of the ship self-defense systems against air threads and detailed information about littoral warfare operations.

CIWS are usually consisting of multi-barrel rapid fire guns, anti-air missiles, jamming antennas, chaff fire mechanisms with the radars and computer support from the functional background. When an incoming missile is sensed by radars, common behavior of autonomous CIWS is as follows. First, algorithms in computers estimate the trajectory of the incoming thread. Then accordingly, rotary rapid guns fire bullets to the path of the thread to make the missile crash. At the same time, either jamming antennas send powerful signals, or chaffs/decoys are fired, or even both, to mislead and invalidate the seeker of the thread. If still danger does not pass, anti-air missile is launched to shot down the incoming missile. These all defense mechanisms mostly achieve to success if there is enough time for the CIWS to react. In Figure 1.1, examples of some CIWS defense systems can be seen on field.

Figure 1.1 : CIWS on Field; Anti-Air Missile, Rapid Gun Fire and Chaff Firing

In the thesis [3], which is published in 1994, Schulte has analyzed the effectiveness of anti-ship missiles against ships with the historical data of several anti-ship missiles up to that year. In Table 1.1, results of his detailed analysis are shown.

Table 1.1 : Probability of Hit by Category

	Total Probability of Hit	Post 1982 Probability of Hit
Defenseless Target	0.913	0.981
Defendable Target	0.684	0.630
Defended Target	0.264	0.450

From the results, two consequences can be deducted. First, possessing and using a defense system for ships is very crucial, defended targets are much more likely to survive. Second, from the statistics of the post 1982 data, it is seen that even target ship is defending; anti-ship missiles achieving to success are more than the ones of the previous era. This result is mostly due to developments in control strategies of the anti-ship missiles against counter systems of the warships, which makes these strategies also crucial for missiles. Therefore, in today's world, anti-ship missiles use wide variety of guidance and control strategies during their flight in order to maximize their probability of hitting to the targeted ship.

1.1 Anti-Ship Missile and Sea Skimming Guidance Concept

Most generally, anti-ship missiles are cruise missiles having the ability of reaching ranges over 200 km and flying more than 15 minutes. Such a long fly time compared to other missiles like anti-tank or anti-air missiles, obviously, brings very complicated control strategies. The mission of an anti-ship missile starts with route planning even before launch phase. After launching, missile adopts distinctive guidance methods for each phase of the flight. And finally, at the end game, missile again uses several tactics for different engagement conditions to hit the target.

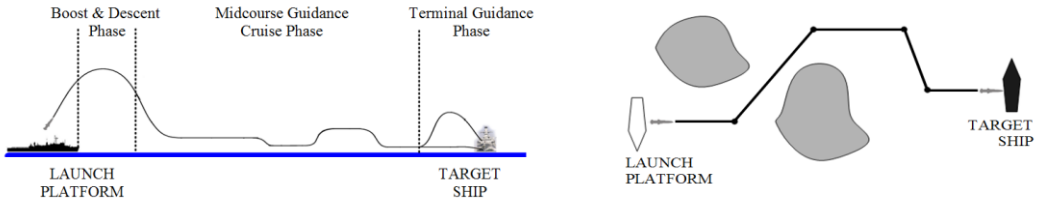

(a) Altitude Profile (b) Trajectory

Figure 1.2 : Sample Mission Profile for an Anti-Ship Missile

In Figure 1.2, a sample mission profile for an anti-ship missile is shown. For the vertical plane, altitude profile is mainly divided into three different phases, which are; boost and descent phase, midcourse guidance phase and terminal guidance phase. Similarly, horizontal plane flight phases involve; initial maneuver, midcourse guidance phase and terminal guidance phase. To be more precise, these phases can briefly be explained as follows.

Before launch, target location is marked with the information taken either from the radar signals of the own platform, or from an outside source. Then, mission planning algorithm runs and produces an optimal path plan for the missile by considering several considerations. Major deliberations for the mission profile algorithm can be sorted as, time-to-go minimization, detectability and radar cost, fuel optimized range maximization and desired engagement geometry. In [4] and [5], one can find detailed and satisfactory information about path planning.

After launching, initial maneuver guidance forces the missile to hold the desired path in yaw channel, while in pitch channel, a descent algorithm drives the missile to the sea skim altitude. During the long midcourse guidance phase, missile follows the trajectory dictated by the mission plan algorithm in order to avoid islands, lands and other allied forces. Trajectory is generally provided to the missile as waypoints to be passed. In [6], [7] and [8] different waypoint guidance methods are explained in detail. While tracking the waypoints in yaw channel, missile is flown just over the mean sea level in pitch channel, at differing altitudes which depend on the condition of the sea and geography.

Finally, when the remaining range comes down to a value smaller than the pre-determined threshold, seeker is turned on and target is acquired. At this terminal guidance phase, missile should adopt intelligent strategies to overcome the defense systems of the target ship. In [9], [10] and [11] one can find the details of different terminal guidance control strategies for an anti-ship missile for the end game trajectory.

For the midcourse guidance cruise phase in pitch channel, anti-ship missiles have long been using sea skimming guidance in order to remain under radar horizon of the target ship; so that, they avoid detection by target radars. A simple geometry of earth's surface for an engagement scenario of an anti-ship missile and targeted warship can be seen in Figure 1.3.

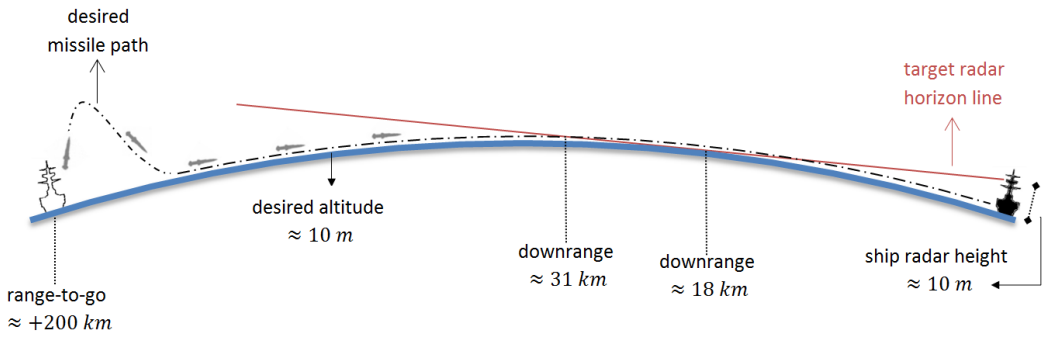

Figure 1.3 : Sea Skimming Guidance and Radar Horizon

As explained previously, battleships possess very effective defense systems against air-attacks. Lower the flight altitude of an anti-ship missile means that longer it takes for the target ship to detect the incoming thread. This late detection yields to the result that battleship will not have enough time to apply counter attacks properly, which is definitely in favor of the missile. Thus, a mission challenge with these missiles is to achieve a smooth height profile just above the mean sea level, throughout the whole midcourse phase, even for some part of the terminal phase. The main focus of this thesis will be the implementation of the sea skimming guidance to an anti-ship missile and validation of the implemented method in every aspect.

1.2 Literature Survey

As already emphasized, powerful defense systems of the battleships opened a road for the effective sea skimming guidance in the past decades. Although there are not hundreds of studies about sea skimming altitude control in the literature, there are definitely a few comprehensive investigations about both how the disturbances affect the flight of the missile negatively and how to overcome these problems.

In 1985, Dowdle [12] proposed an altitude control system design for a supersonic low-altitude missile by using optimal regulatory theory for an ideal simulation. As he already stated in that paper, many additional issues are untouched and should be considered carefully. In his second paper at same conference [13], the problem of implementing a full-state altitude control law by using the Kalman filter estimations is addressed. In that work, while random noise is used as the wave disturbance with a certain root mean square, or shortly RMS, value, other disturbances and sensor errors are not considered. At last, he drew the conclusion that, bandwidth of the Kalman filter is bounded by both transient response requirements and instabilities induced from acceleration command in the stochastic process.

In 1990, Lesieutre et al. [14] analyzed the missiles flying low over various sea states by modeling both the sea wave elevations and unsteady aerodynamics due to air/sea environment. In that paper, authors resulted that missiles flying close to the sea may have control problems for the high sea states. Even the authors emphasize the sea

wave disturbance problem by stating that sea state 5 conditions draws the operational limits for low level flights. In the following work published in 1993, Lesieutre et al. [15] widen the scope of the simulation by adding the rigid/flexible body effect and some sensor errors. The results of that paper are for the high sea states, the missile experiences very large unsteady aerodynamic forces due to disturbances, which actually does not affect the ability of the control system to maintain at low flight altitude over the sea.

In 2002, Talole et al. [16] designed a height control system by using predictive filter which reduces the effect of sea wave disturbance on the missile significantly. In that work, sea wave disturbance is modeled as pure sinusoidal wave and other errors are not taken into account. In their following work in 2011, Priyamvada et al. [17] published a more detailed paper, exactly about the sea skimming altitude control. The authors proposed an extended state observer, or shortly ESO, based height

control system which removes the sea wave disturbances by estimating the exact wave height as an extended state. But the practicality of that method was poor as not taking into account the accelerometer errors and power limitations for flight computer.

In [18] published in 2016, which can be mentioned as the previous study of this thesis, extended Kalman filter, or shortly EKF, based altitude controller is proposed. In that paper, proposed altitude control algorithm shows satisfactory results under the existence of sea wave disturbance, altimeter noise and accelerometer bias. Moreover its feasibility is proved not only in theory but also in practical usage for a digital discrete time computer. The considerations in that paper were almost in every aspect but it does not include a detailed work and some major topic in this thesis like the optimum altitude determination.

Apart from the sea skimming control problem, determination of the optimum flight altitude problem is addressed in [19]. In that document, publisher explains a method to obtain an optimum altitude from the measurements of radar altimeter. More

precisely; first, set of filters and algebraic calculations are applied to altimeter measurements to obtain instantaneous wave height. Then, by comparing the wave height regime with the theoretical and statistical wave heights, an estimate for a safe flight altitude with an acceptable risk is calculated and commanded to the vehicle.

The main difference between this study and the ones already in literature is to optimize the sea skimming flight of the anti-ship missile by means of both altitude controller and altitude commander together, with considering all the disturbances and conditions at the same time. By this way, proposed method provides more robustness against many practical problems.

1.3 Contribution of this Thesis

The problem with the sea skimming guidance is that flying at very low altitude above mean sea level is very risky. Missile should fly smoothly and follow the desired altitude command precisely; otherwise, ditching into sea is inevitable. Furthermore, determination of the flight altitude is another thing to consider. As already mentioned, lowering the flight altitude even a few meters, is invaluable for the survival of the missile at the end game. But the question is, as the flight altitude lowers, the risk of ditching into sea increases which is clearly not preferred. Thus, an optimization of the flight altitude should be performed for the instantaneous flight condition. Having stated the problems, before designing the altitude controller, designer should choose the altitude feedback for the controller properly.

One feedback mechanism can be thought as the solution of the navigation algorithm. Inertial navigation systems, or shortly INS, are used in almost all flight vehicles to calculate the position, velocity and orientation of the vehicle at each instant by using the data from accelerators and gyros. But it is very well known that, these inertial sensors have some bias values on their measurements which definitely makes the navigation solution to drift with time. Although this drift may not be a fatal problem for the vehicles flying at very high altitude, it is definitely crucial for a sea skimming missile. Even with the integration of the global positioning system, or shortly GPS, navigation solution is still not satisfactory enough to be used in altitude control of an

anti-ship missile, since the accuracy of the GPS receivers in altitude channel are at the order of 10 meters.

Other feedback mechanism is the altimeters for altitude measurements, specifically the radar altimeter, which is a very common choice for an anti-ship missile to be used in altitude control loop. Radar altimeter measures the actual height from sea surface rather than the height above mean sea level. This phenomenon causes the sea waves to act directly as a disturbance to altitude control system and can be crucial for missile under bad weather conditions; since, the change in wave height increases significantly. Moreover, independently from sea wave disturbance, radar altimeter measurements are noisy by its nature, like any other sensor output. This may push designer not to use these measurements directly; instead, designer may want to either filter the measurements or estimate height by aiding the altimeter measurement with another sensor, specifically with accelerometer in this study. Filtering altimeter data is not a solution in most cases since the bandwidth requirements will be very low which cause the filter to suppress noise also with the missile motion. On the other hand, sensor fusion with accelerometer also brings problems due to accelerometer errors, mainly due to its bias and the noise characteristics.

In brief, while navigation solution is not noisy but drifted, altimeter data is noisy but not drifted. The idea is to merge these two data to achieve a noise free and not drifted altitude feedback, in order to control the height of the sea skimming missile.

All in all, in this thesis a comprehensive application of Kalman filter is applied in order to achieve a smooth height profile. In this study, disturbances due to weather conditions, sea surface elevations and sensor errors are considered as well as the applicability of the proposed method practically. Moreover, determination of an optimum flight altitude algorithm is proposed which assures the missile to adopt itself to the state it is in. Finally, results of the proposed method for every possible case is shared and compared with the results of the previous approaches to this problem in literature.

1.4 Thesis Structure

In the first chapter, a brief introduction about the battleships and their self-defense mechanisms, anti-ship missiles and their control strategies, specifically sea skimming guidance concept, is given. Then contribution of this thesis is shared and a literature survey about the very specific topic of this thesis is performed.

The second chapter is called modeling of sea wave disturbance. In this chapter, detailed information and different approaches for modeling sea surface elevations is provided. Definition of sea state is made and its use in literature is mentioned. For a high fidelity of sea skimming missile simulation, sea wave disturbance is modeled as well as with its effect as wave gusts.

The third chapter involves the modeling of the whole missile by means of aerodynamic characteristics, acceleration autopilot design, and altitude controller design. Starting with the aerodynamic coefficients, linear missile model for pitch plane is obtained. Then, acceleration autopilot is designed for the related flight condition. After that, altitude control loop is closed upon the acceleration autopilot. Finally, some real world effects are introduced to the ideal system and results are analyzed.

In the fourth chapter; first, previous approaches about robust altitude control strategies is analyzed in detail, then the novel method is proposed. Comparative simulation results are shared for various scenarios and discussion is made.

In fifth chapter, statistical approach for sea surface is introduced. Determination of the optimal altitude is performed and explained in detail. Finally, simulation results are shared for the optimal altitude calculation algorithm which is also integrated with the robust altitude controller for different conditions and design parameters.

Finally, in chapter six, thesis is concluded.

CHAPTER 2

MODELING OF SEA WAVE DISTURBANCE

Modeling of sea waves has been being drawn considerable interest among several engineering disciplines through the last decades. Although basic answers to the questions how and why the sea waves occur, how ocean currents behave, are known, many real world applications involving sea waves are in need of taking into account sea wave models numerically while in design phase. For a ship designer, evaluation of sea loads and motions acting on the ship is a crucial part of the design. Same case applies for an offshore wind turbine design process. Wind generated sea wave models are also used in weather forecasting applications. As seen, modeling of sea waves is a completely another discipline and an area of research itself. In the case of this study, in order to analyze the effects of sea waves on the performance of sea skimming missile, a proper model should definitely be built.

Disturbance originating from sea waves on a sea skimming missile reveals itself through two possible channels. First, sea wave elevations, which change with time and space, are measured by radar altimeters reluctantly, which results a noisy altimeter data. Second, airflow near the sea surface is not uniform because of elevating and descending wave motion, which disturbs the airflow around the sea skimming missile. So, in this chapter of the thesis, disturbance due to sea wave elevations will be modeled and will be integrated to missile model later.

2.1 Sea State Definition

Sea state defines the general condition of the sea surface at a certain location and moment. Statistics about sea surface like the wave height, period and power spectrum characterizes the sea state. In oceanographic theory, there are different yet

similar sea state and wave relations under the influence of wind [20]. World Meteorological Organization (WMO) definition of the sea state is the one commonly used. The other common description scales are by Beaufort and Douglas. But the most comprehensive and rooted one is the NATO sea state description, which will also be used in this study. Table 2.1, taken from [21], shows the relation between sea state number and wave properties like significant wave height and wave period under different wind conditions.

Table 2.1 : NATO Sea State Numeral Table for the Open Ocean North Atlantic

Sea State Number	Significant Wave Height (H_s) [m]		Sustained Wind Speed [knots]		Modal Wave Period (T) [sec]		Percentage Probability of Sea State
	Range	Mean	Range	Mean	Range	Mean	
0-1	0 – 0.1	0.05	0 – 6	0.5	-	-	0
2	0.1 – 0.5	0.3	7 – 10	3.5	3.3 – 12.8	6.5	7.2
3	0.5 – 1.25	0.88	11 – 16	8.5	5.0 – 14.8	7.5	22.4
4	1.25 – 2.5	1.88	17 – 21	19	6.1 – 15.2	8.8	28.7
5	2.5 – 4	3.25	22 – 27	24.5	8.3 – 15.5	9.7	15.5
6	4 – 6	5	28 – 47	37.5	9.8 – 16.2	12.4	18.7
7	6 – 9	7.5	48 – 55	51.5	11.8 – 18.5	15	6.1
8	9 – 14	11.5	56 – 63	59.5	14.2 – 18.6	16.4	1.2
>8	> 14	> 14	> 63	>63	15.7 – 23.7	20	<0.05

2.2 Wave Definition and Formulation

Sea wave motion occurs basically due to wind influence. Wave elevations for a certain point depend on the speed, direction and duration of the wind as well as the depth of the related region. Sea surface waves have mainly two frequency components. These are small amplitude and high frequency waves, which are also called wind waves, and the bigger waves which actually specifies the wave height, which are called swells. Figure 2.1 shows the wind and swell component of a sea wave.

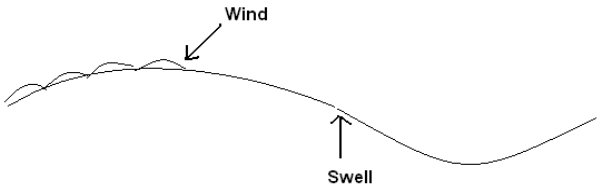

Figure 2.1 : Sea Surface Wave Components

Sine function basically defines the instantaneous height of the regular wave, with a known amplitude ζ, wavelength λ and period T.

$$h_w(x,t) = \zeta \sin\left(\frac{2\pi}{T}t - \frac{2\pi}{\lambda}x\right) \tag{2.1}$$

Angular frequency and wavenumber can be derived from period and wavelength values of a certain wave.

$$\begin{aligned} \omega &= \frac{2\pi}{T} = angular\ frequency \\ k &= \frac{2\pi}{\lambda} = wavenumber \end{aligned} \tag{2.2}$$

Then the equation (2.1) simplifies to;

$$h_w(x,t) = \zeta \sin(\omega t - kx) \tag{2.3}$$

Irregular waves can be considered as the superposition of infinitely many waves with certain amplitudes, wavelengths periods and directions. Figure 2.2 taken from [22] illustrates how a sea surface model can be constructed with series of sine waves.

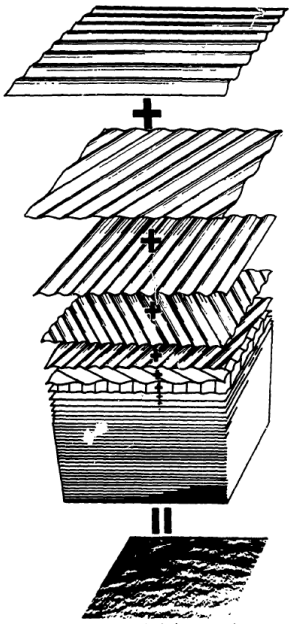

Figure 2.2 : Sum of Many Sine Waves Makes a Sea

In the light of this information, for an irregular sea surface propagating along $+x$ direction, wave elevation can be written as the sum of a large number of wave components with uniformly distributed random phase angles ϕ.

$$h_w(x,t) = \sum_{i=1}^{N} \zeta_i \sin(\omega_i t - k_i x + \phi_i) \tag{2.4}$$

Amplitude of the wave component ζ can be expressed by a wave spectrum $S(\omega)$as stated in [23], where $\Delta\omega$ is a constant difference between successive frequencies.

$$\begin{aligned} \frac{1}{2}\zeta_i^2 &= S(\omega_i)\Delta\omega \\ \zeta_i &= \sqrt{2S(\omega_i)\Delta\omega} \end{aligned} \tag{2.5}$$

Combining the equations (2.4) and (2.5) results the wave elevation function for a certain point in x direction for a certain time instant.

$$h_w(x,t) = \sum_{i=1}^{N} \sqrt{2S(\omega_i)\Delta\omega} \times \sin(\omega_i t - k_i x + \phi_i) \tag{2.6}$$

There are different yet similar approaches in literature for wave spectrum function $S(\omega)$. Generally, recommended sea spectra from ITTC (International Towing Tank Conference) and ISSC (International Ship and Offshore Structures Congress) are used to calculate wave spectrum. In 1963, a wave spectral formulation for wind generated fully developed seas is developed by Pierson and Moskowitz from analyses of wave spectra in the North Atlantic Ocean [24]. Later in 1978 ITTC and ISSC have recommended the use of a modified version of the Pierson-Moskowitz spectrum as stated in [25], which will also be used as the wave spectrum function for this study.

$$S(\omega) = C_1\omega^{-5} \times \exp(-C_2\omega^{-4})$$
$$C_1 = 487 \times \frac{H_s^2}{T^4} \qquad C_2 = \frac{1949}{T^4} \tag{2.7}$$

In equation (2.7) H_s, sometimes also denoted as $H_{1/3}$, is the significant wave height, which is defined as the mean of the one-third highest waves. The parameter T, on the other hand, stands for the modal wave period of the sea state.

For a certain sea state, from Table 2.1 one can read the significant wave height and modal wave period, and thus, can obtain the wave spectrum function. A schematic, illustrating the connection between a frequency domain and time domain representation of waves given in [23], is also shared here in Figure 2.3.

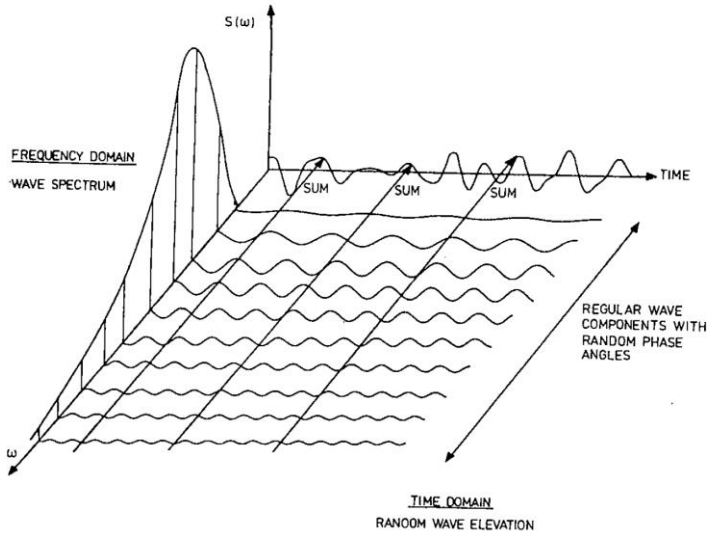

Figure 2.3 : Frequency and Time Domain Representation of Waves

This spectrum results with the long-crested sea surface model, as can be seen in Figure 2.4.

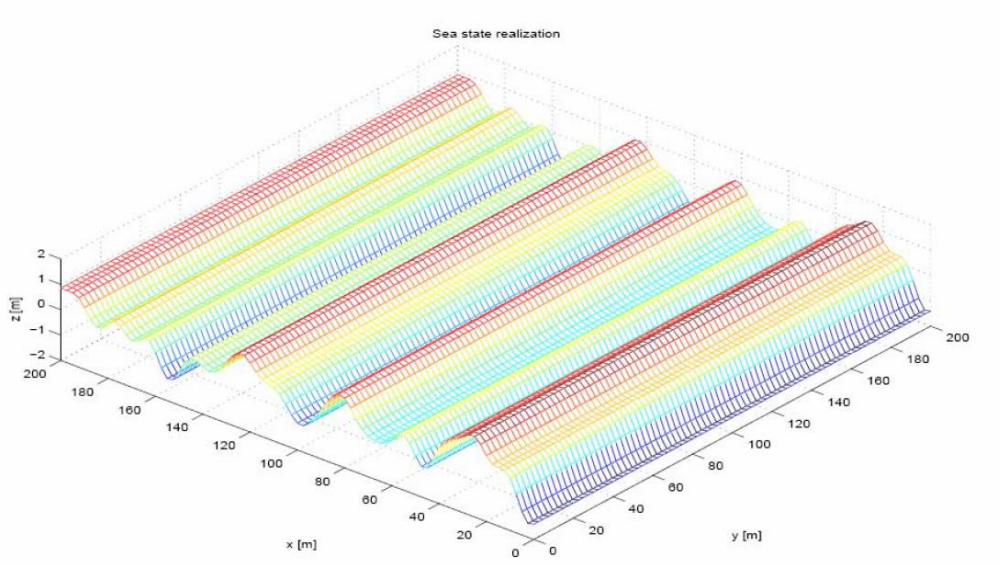

Figure 2.4 : Long-Crested Sea Surface

Here, the missing part is the directional spreading of sine waves. More realistic sea surface model can be obtained by making the wave spectrum function as two dimensional, i.e., function of direction as well. An example of a directional spreading function is given in [23].

$$D(\psi) = \frac{2}{\pi}\cos^2(\psi - \psi_0) \tag{2.8}$$

In equation (2.8), ψ is the direction of the individual wave component whereas ψ_0 is the main wave propagation direction, which can be considered as the same with the sustained wind direction. After this addition, wave spectrum function takes the form given in equation (2.9).

$$S(\omega,\psi) = S(\omega) \times D(\psi)$$
$$S(\omega,\psi) = \left[487\frac{H_s^2\omega^{-5}}{T^4} \times e^{\left(-\frac{1949\omega^{-4}}{T^4}\right)}\right] \times \left[\frac{2}{\pi}\cos^2(\psi - \psi_0)\right] \tag{2.9}$$

With the addition of the directional spreading, short-crested sea surface is now obtained as can be seen in Figure 2.5.

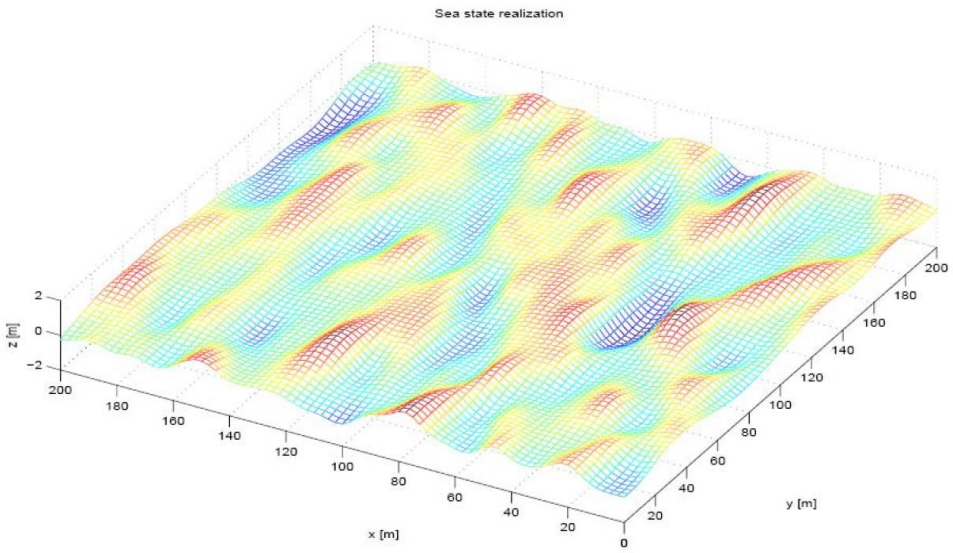

Figure 2.5 : Short-Crested Sea Surface

Finally, wave elevation at certain point (x, y), at a certain time (t) can be calculated with many individual wave components as in the equation (2.10).

$$h_w(x,y,t) = \sum_{i=1}^{M}\sum_{j=1}^{N}\left\{\sqrt{2S(\omega_i,\psi_j)\Delta\omega\Delta\psi} \times \sin\left(\omega_i t - k_i x\cos\psi_j - k_i y\sin\psi_k + \phi_{ij}\right)\right\} \tag{2.10}$$

The parameter k in the equation (2.10), wavenumber, was already defined previously in equation (2.2). However, there exists a much more proper approach for wavenumber, for a free-surface condition in [25], which is called *dispersion relation*.

$$\omega_i^2 = k_i\, g \tanh(k_i d) \tag{2.11}$$

In equation (2.11), g is the gravity, d is the water depth. For infinite depth water, that is $d/\lambda > 1/2$, equation (2.11) simplifies to equation (2.12) since hyperbolic tangent function approaches 1 as depth value goes to infinity. Depth for the open oceans can be assumed infinite easily, thus, for this study simplified equation (2.12) will be used for the wavenumber calculation.

$$k_i = \frac{\omega_i^2}{g} \tag{2.12}$$

In order to finalize the sea surface model frequency and direction arrays which will be used in equation (2.10) should be determined. In [25], it is suggested that to use at least 1000 wave components for a good realization of a sea surface. Thus, choosing M and N as 35 provides 1225 wave components, which will be enough. Among these 1225 wave components, there will be both high and low energy components. Low energy components are the ones which have very high frequencies, i.e., far from the dominant frequency of the related sea state, and the ones whose direction is far from the main wave propagation direction. So, in order not to bother to calculate low energy components, frequency and direction intervals should also be chosen properly.

For the frequency interval, a cut of frequency is defined as the three times of the peak frequency of the related sea state. Then, frequency array can be constructed, with a range of frequencies linearly spaced from incremental frequency to the three times of the peak frequency.

$$\Delta\omega = \frac{3\omega_{peak}}{M}$$
$$\bar{\Omega} = [\Delta\omega \quad 2\Delta\omega \quad \cdots \quad \omega_{peak} \quad \cdots \quad 3\omega_{peak}] \tag{2.13}$$

On the other hand, boundaries of the direction interval can be chosen easily as the minus and plus 90 degrees to the main wave propagation direction.

$$\Delta\psi = \frac{\pi}{N}$$
$$\bar{\Psi} = \left[\psi_0 - \frac{\pi}{2} + \Delta\psi \quad \cdots \quad \psi_0 \quad \cdots \quad \psi_0 + \frac{\pi}{2} - \Delta\psi\right] \tag{2.14}$$

All in all, for each individual wave component, wave spectrum function can be obtained and is ready to be used in wave elevation formula. In Figure 2.6 a sample wave spectra for sea state 4 can be seen. As expected, the components near to the peak frequency and with no directional spreading have the highest energy, while the components far from the peak frequency and main wave propagation direction have lower energy.

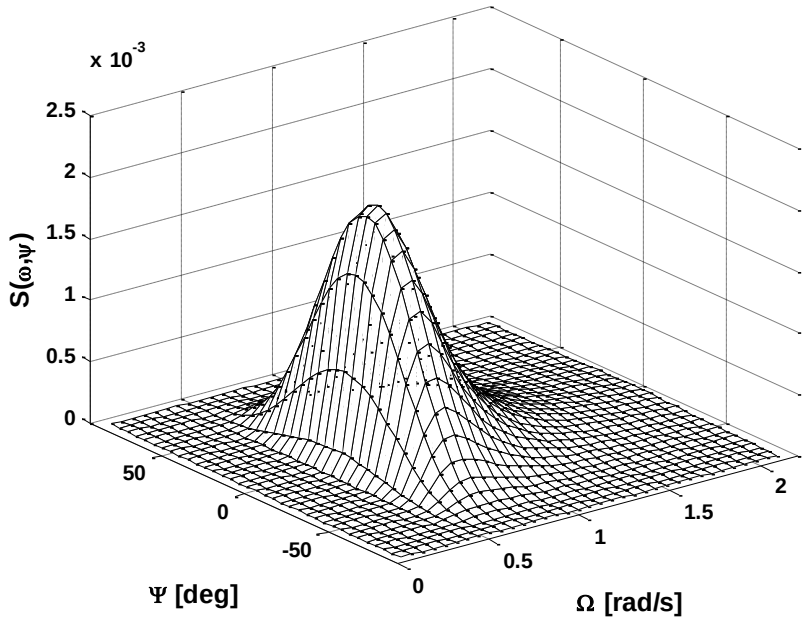

Figure 2.6 : Wave Spectra

2.3 Gust Disturbance due to Sea Surface Elevation

Cruise altitude for sea skimming missiles is generally less than 20 meters over mean sea level. At this much low altitude, the airflow over the sea surface is not uniform, especially when high sea states causing 5m-height wave elevations are considered. The distorted airflow can be modeled as a gust disturbance which acts as an unsteady forcing function on the missile during its flight.

In [15], it is stated that the vertical gust occurs with a 90-degree phase shift with respect to the wave sinusoidal. So, using cosine function instead of sine function in wave model, will realize the gust behavior. Moreover, magnitude of the vertical gust velocity due to wave plunging motion as a function of altitude can be obtained from the solution of the wave equation.

$$v_g = \zeta \cos(\omega t - kx \cos\psi - ky \sin\psi + \phi)\, f U_w e^{-fh} \tag{2.15}$$

In equation (2.15), $f = 2\pi/\lambda_w$ and U_w is the wind velocity, which can be assumed to be same with the wave propagation speed since fully developed sea conditions are

considered. In order to get rid of the parameter f , manipulating the equation (2.15) a bit, since $\lambda_w = U_w T$, results with the equation (2.16), in which all parameters are already known from our previous study of sea wave modeling.

$$v_g = \zeta \cos(\omega t - kx\cos\psi - ky\sin\psi + \phi)\,\omega_p e^{-\frac{\omega_p}{U_w}h} \tag{2.16}$$

In equation (2.16) ω_p is the peak frequency of the related sea state and h is the altitude of the missile. Note that, exponential factor in the formula provides gust velocity approach zero and airflow to be uniform as the missile fly at higher altitudes.

As in the wave elevation model, using the same individual wave components provides a realistic gust disturbance model;

$$\begin{aligned} v_g(x,y,t) = \sum_{i=1}^{M}\sum_{j=1}^{N}\Bigg\{ & \sqrt{2S(\omega_i,\psi_j)\Delta\omega\Delta\psi} \\ & \times \cos(\omega_i t - k_i x\cos\psi_j - k_i y\sin\psi_k + \phi_{ij})\Bigg\} \times \omega e^{-\frac{\omega}{U_w}h} \end{aligned} \tag{2.17}$$

Considering the missile is flying at sea skim altitude with nearly zero roll and pitch angles, vertical gust disturbance can also be considered as angle of attack disturbance for the missile as in equation (2.18).

$$\alpha_{gust} = \tan\left(\frac{v_g}{U_{missile}}\right) \approx \frac{v_g}{U_{missile}} \tag{2.18}$$

CHAPTER 3

MISSILE MODEL AND ALTITUDE CONTROL DESIGN

In this chapter, whole design process of the ideal altitude controller will be explained stage by stage. First, missile model is constructed and presented with block diagrams. Then, acceleration autopilot is designed to control the longitudinal dynamics of the missile by means of acceleration command and response. After that, height control system is closed upon the acceleration autopilot to control the altitude of the vehicle. Simulation results will be shared for the designed height control system under several conditions. Investigation of the results will show that, although height control system is working very well for the ideal cases, it will turn out to be the performance of the designed height controller is unsatisfactory for the realistic simulation conditions.

3.1 Missile Model

Since, the concern of this study is altitude control, modeling the pitch plane motion will be sufficient for the analyses. A sample missile schematic shown in Figure 3.1 illustrates the pitch plane motion related parameters for the missile.

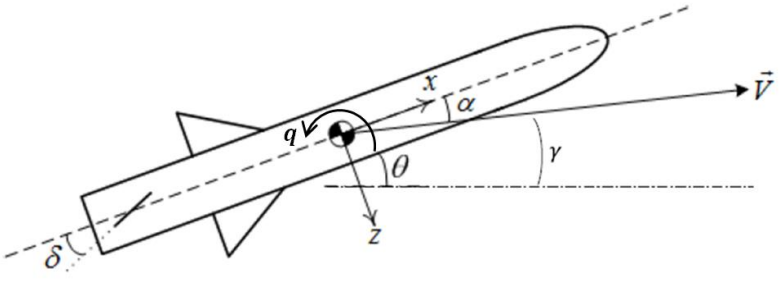

Figure 3.1 : Missile Coordinate System and Parameters

Detailed derivation of equations of motion for a flying vehicle is shared in APPENDIX A. Moreover, linearization of equations of motion for pitch plane is performed in APPENDIX B. For this study, dynamics for pitch plane will be expressed as LTI (Linear Time Invariant) system. Linearized dynamics for pitch plane, for a general missile can be written in state space form as in the equation (3.1).

$$\begin{gathered} \dot{x} = Ax + Bu \\ \begin{bmatrix} \dot{\alpha} \\ \dot{q} \end{bmatrix} = \begin{bmatrix} \frac{Z_\alpha}{V} & \frac{Z_q}{V} + 1 \\ M_\alpha & M_q \end{bmatrix} \begin{bmatrix} \alpha \\ q \end{bmatrix} + \begin{bmatrix} \frac{Z_\delta}{V} \\ M_\delta \end{bmatrix} [\delta] \\ y = Cx + Du \\ a_z = [Z_\alpha \quad Z_q] \begin{bmatrix} \alpha \\ q \end{bmatrix} + [Z_\delta][\delta] \end{gathered} \tag{3.1}$$

In equation (3.1) α is the angle of attack, q is the pitch angular rate, δ is the control surface deflection, a_z is the acceleration of body in z-direction. Block diagram of the given LTI system is shown in Figure 3.2.

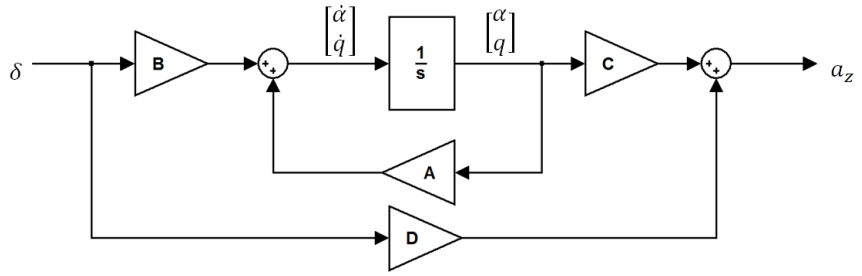

Figure 3.2 : Block Diagram of the Pitch Plane LTI System

Input to the LTI system is the control surface deflection angle δ as stated earlier. Control surface deflection is realized by a CAS (Control Actuation System) for a desired fin angle δ_{com}. CAS has its own dynamics which can be represented by a second order transfer function with a proper natural frequency and damping ratio as in the equation (3.2).

$$\frac{\delta}{\delta_{com}}(s) = \frac{\omega_n^2}{s^2 + 2\zeta\omega_n s + \omega_n^2} \tag{3.2}$$

$$\omega_n = 20Hz \quad ; \quad \zeta = 0.8$$

Then, considering LTI system given in equation (3.1) and CAS in equation (3.2) together, the block diagram in Figure 3.3 is obtained.

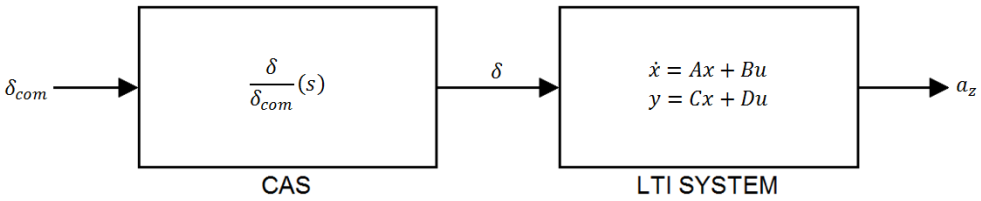

Figure 3.3 : Block Diagram of the CAS and LTI System

In order to simulate the system, numerical values of missile aerodynamic and geometric parameters are needed. In [26], which is a study about performance analyses for an anti-ship missile, aerodynamic stability derivatives with the geometrical and inertial properties are provided for a cruise missile. Those parameters will also be used for this study and can be seen in Table 3.1.

Table 3.1 : Aerodynamic, Geometric and Inertial Parameters for a Cruise Missile

Aerodynamics Stability Derivatives (for Mach = 0.8)	
C_{Z_α}	$-20.5\ [1/rad]$
C_{Z_δ}	$-7.2\ [1/rad]$
C_{M_α}	$-24.6\ [1/rad]$
C_{M_δ}	$-33.2\ [1/rad]$
Geometric & Inertial Properties	
S_{ref}	$0.092\ [m^2]$
l_{ref}	$0.343\ [m]$
m	$500\ [kg]$
I_{yy}	$500\ [kgm^2]$

By using non-dimensional aerodynamic stability derivatives and geometric and inertial properties, dimensional aerodynamic derivatives with the notation given in (B.10) is obtained and shared in Table 3.2.

Table 3.2 : Dimensional Aerodynamic Derivatives

$Z_\alpha = Cz_\alpha \frac{QS_{ref}}{m}$	-170.93
$Z_\delta = Cz_\delta \frac{QS_{ref}}{m}$	-60.03
$M_\alpha = Cm_\alpha \frac{QS_{ref}l_{ref}}{I_{yy}}$	-70.35
$M_\delta = Cm_\delta \frac{QS_{ref}l_{ref}}{I_{yy}}$	-94.95

The input to the system in Figure 3.3 is the control surface deflection command δ_{com}, which will be produced by the autopilot. Main focus of this study is altitude controller, which will be closed on an inner loop autopilot. In literature, different kinds of autopilots are used as inner loop for the height control systems. In [27], analyses for height control loop of cruise missile is performed for both attitude and acceleration autopilot. Both autopilots have their own advantages and drawbacks. But, acceleration autopilot is much favorable because of the fact that ease of gravity compensation, thus acceleration autopilot is used in this study as an inner loop stabilizer for the altitude control system.

3.2 Acceleration Autopilot Design

There exist different acceleration autopilot configurations in the literature as well as different design techniques for each configuration. The former study mentioned earlier [26] adopts the pole placement method for the two loop PI controlled autopilot design. In [28], three-loop autopilot is designed for acceleration control with root locus method. Another very well-known autopilot configuration is the full state feedback controller approach given for different applications in [29]. In this study, full state feedback controller will be adapted to acceleration autopilot, and the gains will be calculated by pole placement method.

For the autopilot design, first, system should be written in state space form with all states. In equation (3.1), normal acceleration is not a system state, but the angle of attack is. To obtain a system with normal acceleration as a state, taking the time derivative of the acceleration equation in (3.1) gives (3.3).

$$\dot{a_z} = Z_\alpha \dot{\alpha} + Z_q \dot{q} + Z_\delta \dot{\delta} \tag{3.3}$$

Since the angle of attack is kept in a small interval through the flight, small angle assumption can be made for angle attack and the relation between angle of attack rate and the rate of body velocity is obtained as in equation (3.4).

$$\begin{gathered} \alpha = \operatorname{atan}\frac{w}{u} \approx \frac{w}{u} \approx \frac{w}{V} \\ \dot{\alpha} = \frac{\dot{w}}{V} \end{gathered} \tag{3.4}$$

Also, from the equations of motion derived in APPENDIX B, relation between acceleration and rate of body velocity is known as in equation (3.5).

$$\dot{w} = a_z + qV \tag{3.5}$$

Thus, equation (3.6) is obtained.

$$\dot{\alpha} = \frac{\dot{w}}{V} = \frac{a_z + qV}{V} = \frac{a_z}{V} + q \tag{3.6}$$

Re-writing the acceleration equation in (3.1) gives the relation between angle of attack and acceleration as in equation (3.7).

$$\begin{gathered} a_z = Z_\alpha \alpha + Z_q q + Z_\delta \delta \\ \alpha = \frac{a_z - Z_q q - Z_\delta \delta}{Z_\alpha} \end{gathered} \tag{3.7}$$

Then, substituting the relation obtained in equation (3.7) into the angular rate equation in (3.1) gives the relation in equation (3.8).

$$\begin{gathered} \dot{q} = M_\alpha \alpha + M_q q + M_\delta \delta \\ \dot{q} = M_\alpha \left(\frac{a_z - Z_q q - Z_\delta \delta}{Z_\alpha} \right) + M_q q + M_\delta \delta \end{gathered} \tag{3.8}$$

Substituting (3.6) and (3.8) into (3.3) yields to the following equation;

$$\begin{aligned} \dot{a_z} &= Z_\alpha \dot{\alpha} + Z_q \dot{q} + Z_\delta \dot{\delta} \\ \dot{a_z} &= Z_\alpha \left[\frac{a_z}{V} + q\right] + Z_q \left[M_\alpha \left(\frac{a_z - Z_q q - Z_\delta \delta}{Z_\alpha}\right) + M_q q + M_\delta \delta\right] + Z_\delta \dot{\delta} \\ \dot{a_z} &= \left(\frac{Z_\alpha}{V} + \frac{Z_q M_\alpha}{Z_\alpha}\right) a_z + \left(Z_\alpha - \frac{Z_q^2 M_\alpha}{Z_\alpha} + Z_q M_q\right) q \\ &\quad + \left(Z_q M_\delta - \frac{Z_q M_\alpha Z_\delta}{Z_\alpha}\right) \delta + (Z_\delta)\, \dot{\delta} \end{aligned} \tag{3.9}$$

Also, re-writing (3.8) and modifying gives;

$$\begin{aligned} \dot{q} &= M_\alpha \left(\frac{a_z - Z_q q - Z_\delta \delta}{Z_\alpha}\right) + M_q q + M_\delta \delta \\ \dot{q} &= \left(\frac{M_\alpha}{Z_\alpha}\right) a_z + \left(M_q - \frac{M_\alpha Z_q}{Z_\alpha}\right) q + \left(M_\delta - \frac{M_\alpha Z_\delta}{Z_\alpha}\right) \delta \end{aligned} \tag{3.10}$$

Moreover, transfer function given in (3.2) provides the following relation.

$$\ddot{\delta} = \omega_n^2 \delta_{com} - 2\zeta\omega_n \dot{\delta} - \omega_n^2 \delta \tag{3.11}$$

Finally, open loop system dynamics can be written in state space form by combining the equations (3.9), (3.10) and (3.11) as shown in the equation set (3.12).

$$\begin{aligned} \dot{x} &= Ax + Bu \\ y &= Cx + Du \end{aligned}$$

$$A = \begin{bmatrix} \frac{Z_\alpha}{V} + \frac{Z_q M_\alpha}{Z_\alpha} & Z_\alpha + Z_q M_q - \frac{Z_q^2 M_\alpha}{Z_\alpha} & Z_q M_\delta - \frac{Z_q M_\alpha Z_\delta}{Z_\alpha} & Z_\delta \\ \frac{M_\alpha}{Z_\alpha} & M_q - \frac{Z_q M_\alpha}{Z_\alpha} & M_\delta - \frac{Z_\delta M_\alpha}{Z_\alpha} & 0 \\ 0 & 0 & 0 & 1 \\ 0 & 0 & -\omega_n^2 & -2\zeta\omega_n^2 \end{bmatrix} \tag{3.12}$$

$$B = \begin{bmatrix} 0 \\ 0 \\ 0 \\ \omega_n^2 \end{bmatrix} \quad ; \quad x = \begin{bmatrix} a_z \\ q \\ \delta \\ \dot{\delta} \end{bmatrix} \quad ; \quad u = \delta_{com}$$

$$C = [1 \quad 0 \quad 0 \quad 0] \quad ; \quad D = 0$$

In order to design the full state feedback controller upon the open loop system, all the states need to be available for feedback by either measuring or observing. Acceleration and body angular rate is measured by inertial measurement units (IMU). Control surface position and rate information can be provided by CAS sensors. Thus, full state feedback controller can be applied upon the open loop system obtained as long as the system is controllable. Quick check of the rank of the controllability matrix assures the controllability of the system as in the equation (3.13).

$$\mathcal{C}(A,B) = [B \quad AB \quad A^2B \quad A^3B] \qquad rank(\mathcal{C}) = 4 \tag{3.13}$$

One last thing to consider while designing an autopilot, as a nice to have property, is the introduction of integrator to the acceleration state. In order to eliminate steady state error, integrator will be added to the system in (3.12) and the equation set (3.14) is obtained.

$$x_5 = \int a_{z_{err}} = \int \left(a_{z_{com}} - a_z\right)dt$$

$$\dot{\hat{x}} = \hat{A}\hat{x} + \hat{B}u + \tilde{B}a_{z_{com}}$$
$$y = \hat{C}\hat{x} + Du \tag{3.14}$$

$$\hat{A} = \begin{bmatrix} A_{4x4} & 0_{4x1} \\ -C & 0 \end{bmatrix} \quad ; \quad \hat{B} = \begin{bmatrix} B_{4x1} \\ 0 \end{bmatrix} \quad ; \quad \hat{x} = \begin{bmatrix} x_{4x1} \\ \int a_{z_{err}} \end{bmatrix} \quad ; \quad u = \delta_{com}$$

$$\tilde{B} = \begin{bmatrix} 0_{4x1} \\ 1 \end{bmatrix} \quad ; \quad \hat{C} = [C \quad 0] \quad ; \quad D = 0$$

Aim of the autopilot is to produce proper control surface deflection command δ_{com} to achieve desired acceleration $a_{z_{com}}$. In full state feedback controller, each state is multiplied with a unique gain to achieve this aim, as shown in equation (3.15).

$$u = \delta_{com} = -Kx = -k_1x_1 - k_2x_2 - k_3x_3 - k_4x_4 - k_5x_5 \tag{3.15}$$

For the determination of autopilot gains, pole placement method will be used. Desired closed loop performance of the autopilot inherently determines the pole locations to be placed. Two performance criteria play major role for the closed loop pole locations. First, settling time or bandwidth of the autopilot is needed to be determined. Second, desired percentage of the overshoot should be chosen.

Before choosing the closed loop pole locations, quick check of the open loop system which is obtained in (3.12) is performed to have an idea about the open loop characteristics. Pole-zero map of the open loop system is shown in Figure 3.4.

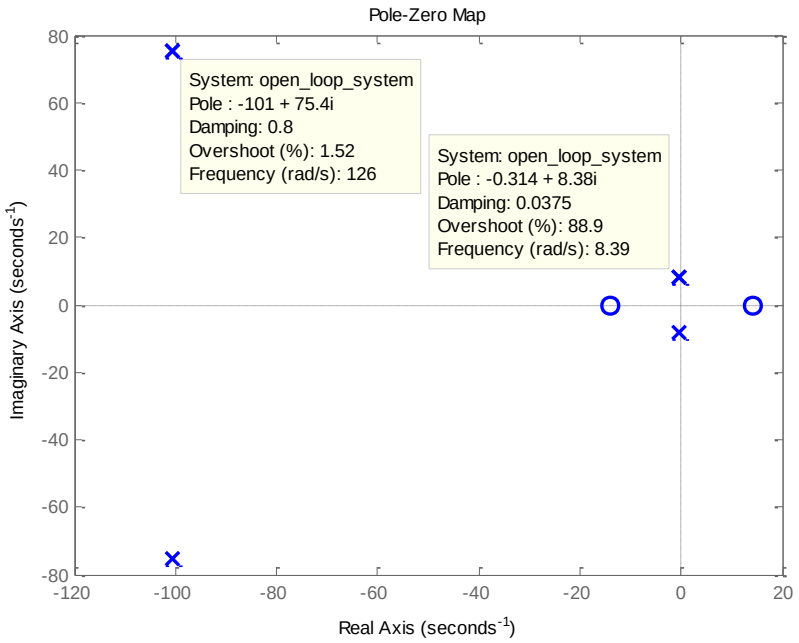

Figure 3.4 : Pole-Zero Map of the Open Loop System

In Figure 3.4, the poles far to the origin belong to the CAS dynamics and they are very fast. On the other hand, the other complex-conjugate pair near the origin, which dominates the system, belongs to the missile open loop characteristics. As seen, open loop characteristics are considerably slow with very low natural frequency and lightly damped with very low damping ratio.

For a sea skimming cruise missile, super-fast autopilot is not a necessity; thus, choosing the desired settling time as 1 second is sufficient. Moreover, overshoot is

not desired for sea skimming missiles because of the very low cruise altitude. Thus, locating the dominant poles with a proper damping ratio to eliminate overshoot and with a proper natural frequency to satisfy settling time will finalize the autopilot design. Choosing the damping ratio of the closed loop dominant poles as 0.8 provides more than enough damping. On the other hand, in order to speed up the system, shifting the dominant open loop poles 14 times to the left satisfy the fast response. The pole which belongs to integral controller is aligned as the same natural frequency with the dominant poles. The poles belonging to CAS dynamics will not be changed. All in all, new pole locations will be as in the equation (3.16).

$$\begin{aligned} p_1 &= -5.5 \\ p_{2,3} &= -4.4 \pm 3.3\, i \\ p_{4,5} &= -101 \pm 75.4\, i \end{aligned} \tag{3.16}$$

Placing these poles will give the desired autopilot gains in equation (3.15). There exist different solutions of obtaining gains by pole placement. One famous method is to use Ackermann's formula [29], which may not be numerically reliable for high order systems. MATLAB command *place* which uses the algorithm in [30] to calculate gain vector numerically, is used in this study to locate desired poles and obtain the gain set in equation (3.17).

$$\begin{gathered} K = place\left(\hat{A}, \hat{B}, [p_1 \quad p_2 \quad p_3 \quad p_4 \quad p_5]\right) \\ K = [-0.0005 \quad -0.1523 \quad -0.1422 \quad +0.0008 \quad -0.0138] \end{gathered} \tag{3.17}$$

Block diagram of the obtained closed loop system is shown in Figure 3.5.

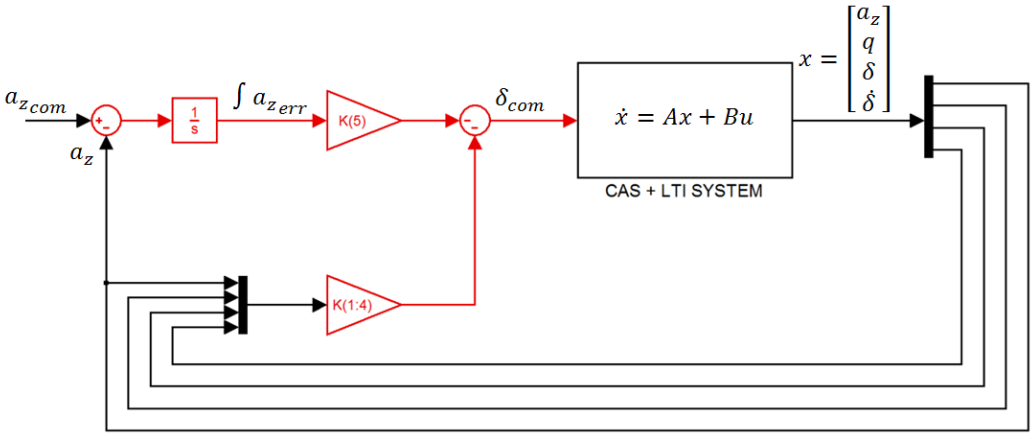

Figure 3.5 : Block Diagram of the Acceleration Autopilot

Also, dominant closed loop pole locations are shown in Figure 3.6 as well as with the dominant open loop poles for comparison.

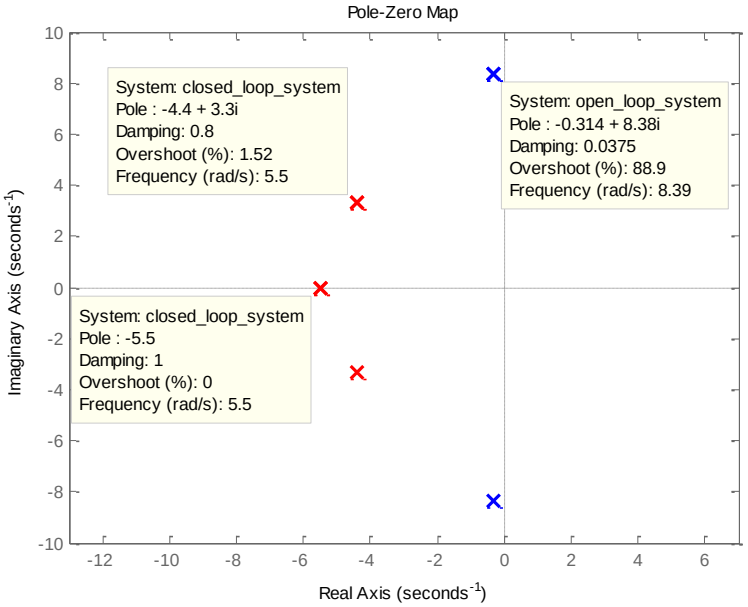

Figure 3.6 : Pole-Zero Map of the Closed Loop System (Acceleration Autopilot)

Moreover, Bode diagram of the closed loop system, with the stability margins highlighted on the graph, is shown in Figure 3.7.

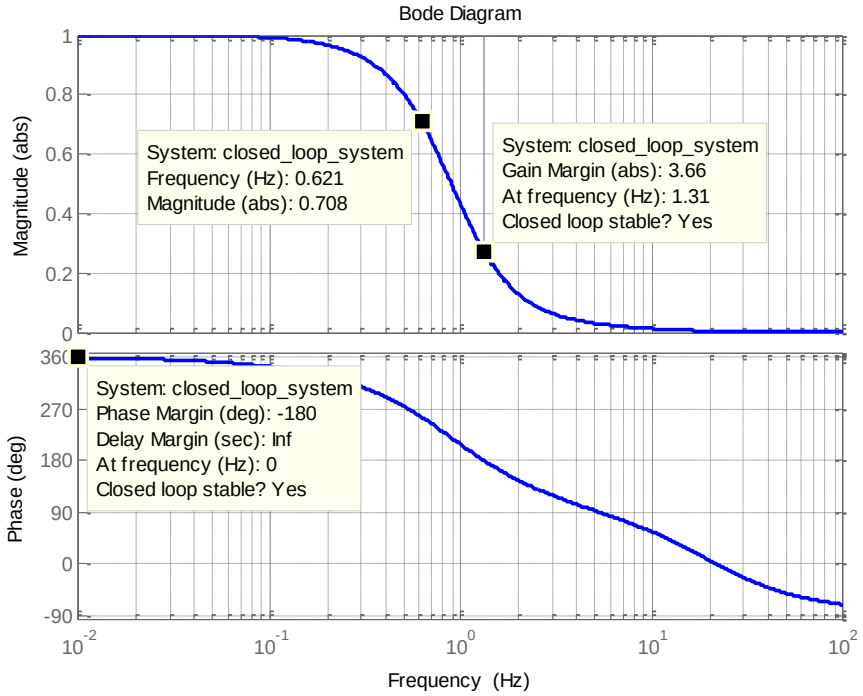

Figure 3.7 : Bode Diagram of the Acceleration Autopilot

Frequency domain analysis of the system can quickly be performed by investigating the Bode diagram. The bandwidth of the system is pointed out on the plot as $0.62\ Hz$, which is defined in [31] as the frequency where the magnitude of Bode diagram falls below $-3dB (\cong 0.708\ abs)$. Closed loop system has gain margin of $11.27\ dB (\cong 3.66\ abs)$ and phase margin of $-180deg$ which are more than enough. These safe margins indicate that, in case of modeling errors and disturbances, system will still be stable and perform as desired.

Finally, Figure 3.8 shows the step response of the acceleration autopilot, with the rise time and settling time shown on the plot. As previously determined, settling time is 1 second and no overshoot is observed, which yields to the result that this autopilot design satisfies the expectations.

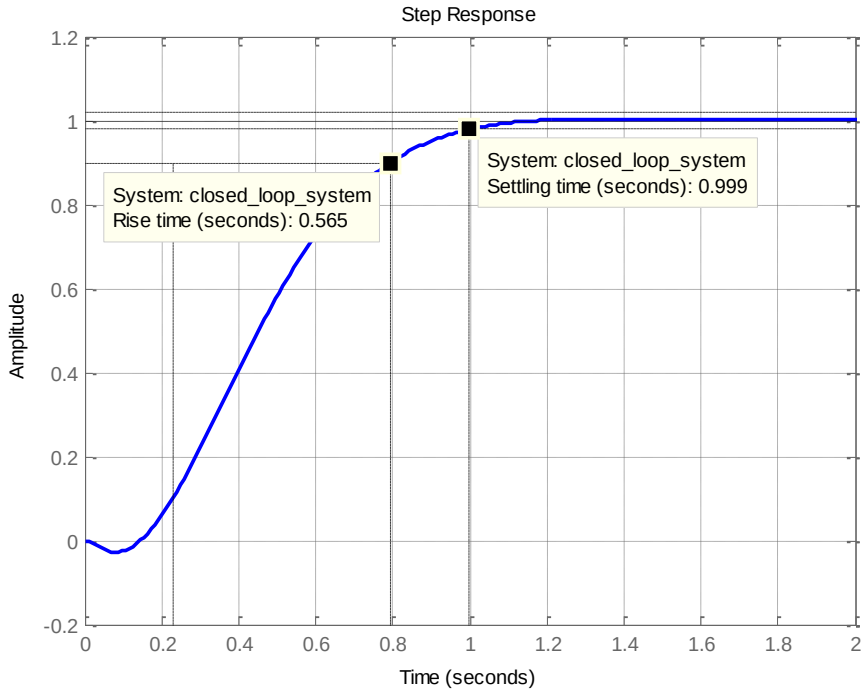

Figure 3.8 : Step Response of the Acceleration Autopilot

3.3 Ideal Case Altitude Controller Design

For the sea skimming phase of the anti-ship missile, an altitude control system is needed. This altitude controller will maintain the cruise altitude of the missile just above the sea surface under the effects of any kind of disturbances and sensor noises.

Having designed the acceleration autopilot, now altitude controller will be closed upon it. Since the level flight is the case, large body angles do not occur, so the relation between the body acceleration and altitude can be represented by a double integration as shown in Figure 3.9.

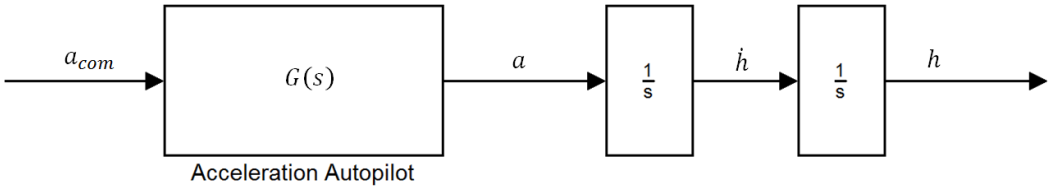

Figure 3.9 : Block Diagram of the Relation between Acceleration and Altitude

Then, transfer function from commanded acceleration to altitude can be written as in the equation (3.18).

$$G(s) = \frac{a}{a_{com}}(s)$$
$$H(s) = \frac{h}{a_{com}}(s) = G(s)\frac{1}{s^2} \tag{3.18}$$

Aim of the altitude controller is to produce proper acceleration command for the autopilot, which will realize that acceleration, in order to achieve desired altitude command. Acceleration autopilot $G(s)$ is a type-0 system. Addition of double integrator makes $H(s)$ a type-2 system. Such a system can be stabilized with a derivative action, by making the system type-1. Thus, proportional and derivative controller (PD) is a proper choice for the altitude controller as an outer loop of acceleration autopilot. Feedback for the controller is provided by the radar altimeter. Since radar altimeter does not measure the altitude over mean sea level, but measures the distance over sea surface just at that moment, instantaneous wave height inherently acts as a disturbance to the system. Block diagram of the altitude controller is shown in Figure 3.10.

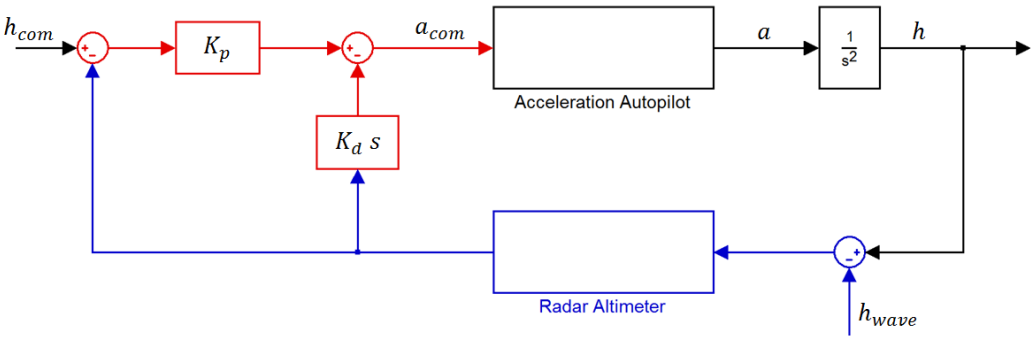

Figure 3.10 : Block Diagram of the Altitude Controller

Proportional and derivative gains now should be set according to the desired performance. For the altitude control action, overshoot is unacceptable since the missile will be flown just over the sea surface. On the other hand, since the subject in this study is a cruise missile, very agile performance is not expected, so relatively slow performance for the altitude control is not a problem. Setting the gains as $K_p = 0.52$ and $K_d = 1.16$ by trial-error, provides a performance with settling time faster than 5 seconds and no overshoot criteria for altitude response. Step response of the altitude controller is shown in Figure 3.11.

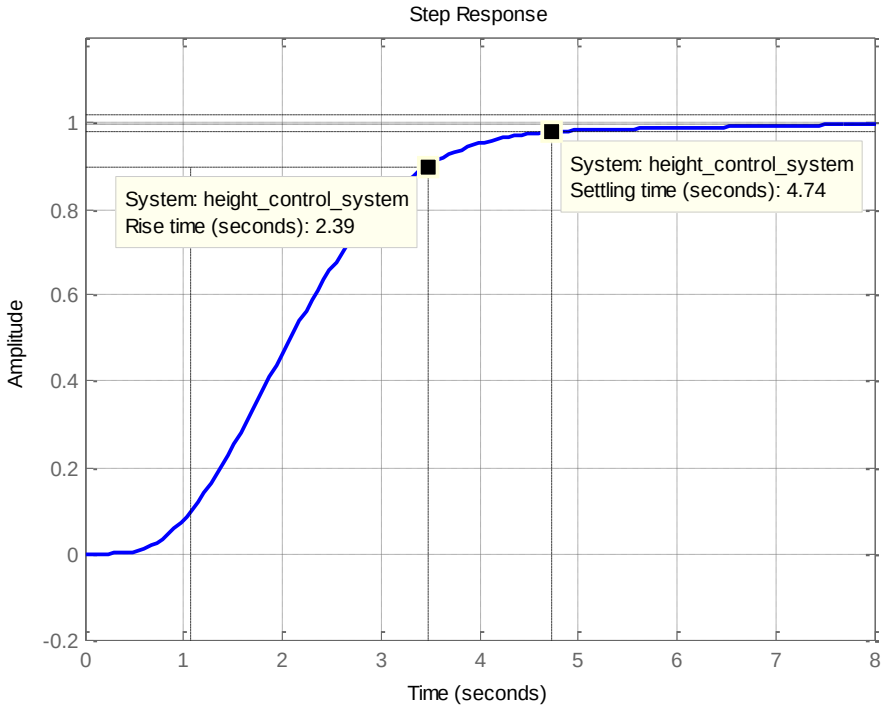

Figure 3.11 : Step Response of the Altitude Controller

After deciding PD controller gains, one can write the transfer function from desired height to achieved height which is shown in equation (3.19). Similarly, considering the sea waves as a disturbance, wave rejection transfer function of the closed loop system can be written as shown in equation (3.20).

$$H_{ClosedLoop}(s) = \frac{h}{h_{com}}(s) = \frac{K_p H(s)}{1 + K_p H(s) + K_d H(s)\, s} \tag{3.19}$$

$$H_{WaveRejection}(s) = \frac{h}{h_{wave}}(s) = \frac{K_p H(s) + K_d H(s)\, s}{1 + K_p H(s) + K_d H(s)\, s} \tag{3.20}$$

Bode diagrams of the closed loop performance transfer function and wave rejection transfer function is shown in Figure 3.12 as well as with the inner loop acceleration autopilot. While the closed loop bode diagram shows performance of the system by means of command tracking, wave rejection bode diagram indicates that system is vulnerable to frequencies of wave components less than 1 Hz.

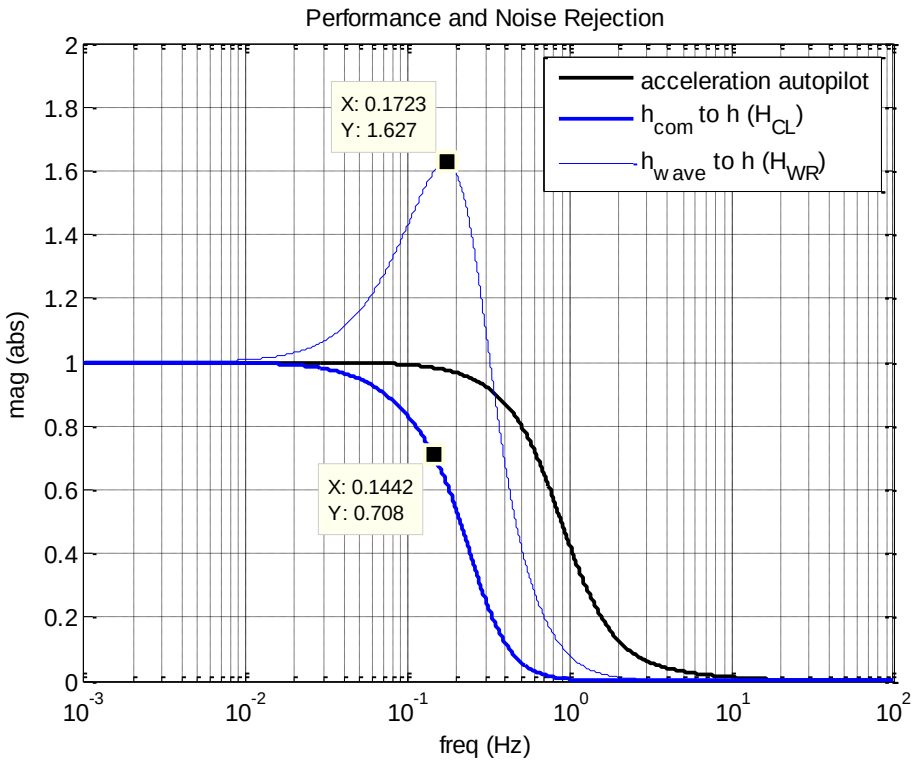

Figure 3.12 : Bode Diagram of the Altitude Control System

3.4 Introduction of Real-World Effects to the System

Performance of the height control system for the ideal feedback case to any input will not be different from the step response shown in Figure 3.11 since linear analysis is performed. On the other hand, performance analyses of the altitude controller should also be performed for realistic cases. Thus, real world effects are introduced into the simulation environment.

3.4.1 Sea Wave Elevations and Radar Altimeter Measurements

Radar altimeter (RA) is the main sensor of the height control system and provides missile altitude and altitude rate data by calculating the time delay between transmitted and received radar signals. Thus, instantaneous sea wave elevations directly act as a disturbance on the measurements. Modeling of the sea wave disturbance has already been explained in detail in CHAPTER 2. Figure 3.13 shows the fast Fourier transform (FFT) graph of the sea wave elevations seen by the missile for sea state 6. There exist considerable amount of frequency components less than 1 Hz which will degrade the system performance as already deducted in previous part.

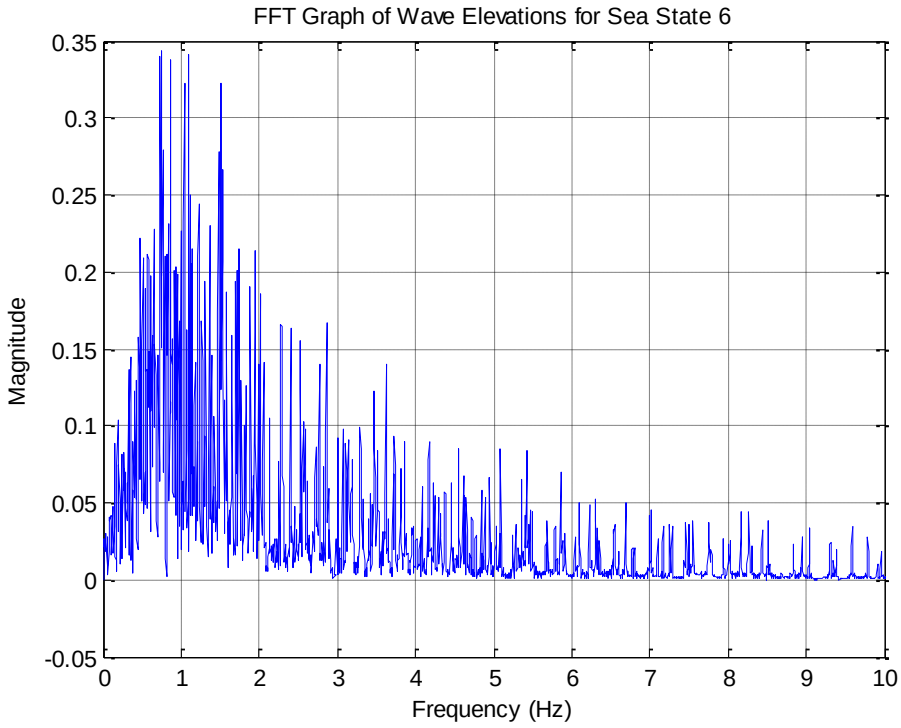

Figure 3.13 : FFT Graph of Wave Elevations for Sea State 6

Moreover, like any other sensors, altimeter has also noises on its measured outputs. Noise of the altimeter can be modeled as a Gaussian distributed white noise, with different variances on two measurements. For this study, RMS values of white noises are taken $3ft(\cong 1m)$ for altitude measurement and $5ft/s(\cong 1.5m/s)$ for altitude rate measurement, as concluded in the information report in [32].

Then, with the sea wave elevations and sensor noises, altimeter measurements can mathematically be expressed as in the equation (3.21).

$$\begin{aligned} h_m &= h - h_w + \eta_h \quad ; \quad \sigma_{\eta_h} = 1m \\ \dot{h}_m &= \dot{h} - \dot{h}_w + \eta_{\dot{h}} \quad ; \quad \sigma_{\eta_{\dot{h}}} = 1.5m/s \end{aligned} \tag{3.21}$$

3.4.2 Inertial Measurement Unit Errors

Inertial measurements units (IMU) are perhaps the most import sensor on air vehicles, which measure the body angular rate and acceleration with respect to inertial frame. These measurements are integrated in inertial navigation systems (INS) in order to calculate the required flight information like position, velocity and orientation of the vehicle at each moment. If those measurements were free of error, then all the flight information would be perfect for the guidance system. Indeed, that is why radar altimeter is needed for the height control system for a sea skimming missile. Although, IMU measurements are not used directly in the height control system, still the error will be modeled to analyze what would have been if the INS altitude feedback was to be used in the height control system.

IMU has different kinds of sensor errors, major examples of which are bias, noise, scale factor and misalignment as stated in [33]. Most effective error source among those is the sensor bias, which causes INS to drift as the time passes since integration process exists in navigation algorithm. Thus, for this study, only the bias error for the accelerometer will be introduced to the system for performance analyses.

Bias error for accelerometers changes in each turn on, which makes the problem non-deterministic. However, accelerometer to be used has its own specifications, stating that bias error will remain in some confidence interval. In the datasheet of HG1700 model IMU of the Honeywell Company [34], which is widely used in missiles and also used in Harpoon anti-ship missile, accelerometer bias for one standard deviation is given as 1 mg. Therefore, for this study, accelerometer bias is taken simply as $0.01\ m/s^2$. Equation (3.22) shows accelerometer measurement equation.

$$a_m = a + a_{bias} \quad ; \quad a_{bias} = 0.01\ m/s^2 \tag{3.22}$$

3.4.3 Limited Computer Power

In control theory, a state can be estimated or observed with the other known states through some algebraic computations. This process is basically done by adjusting observer pole locations or filter gains through some algorithms. In theory, as long as certain conditions are satisfied these algorithms succeeded in estimating. But this may not be the case in real world applications due to several reasons. First of all, theory considers continuous signals; whereas in reality, computers are restricted to work in discrete-time. While the discrete time system approaches continuous time as the time step converges to zero, there is a practical limit to how small the time step can be chosen. Moreover, sensors work in discrete time and output rates are fixed. Thus, for a real-world application, one must choose the observer pole locations or filter gains accordingly.

For this work, missile computer is considered to work in 100 Hz discrete time, and the altimeter and IMU are considered to have measurement rates of the same.

3.5 Simulation Results and Discussion

Having sorted what can the real-world effects be for an altitude control problem of a sea skimming missile, now, performance analyses is performed for each case. Desired height profile for the missile will be 30 meters flyout for first 20 seconds, following with a step command to 10 meters altitude for the rest of the flight.

In Figure 3.14, performance of the altitude controller due only to sea wave disturbance phenomenon is shown for different sea states. Note that sea state 0 condition corresponds to the ideal case. As expected, controller performs just well for the ideal case, while the performance degrades with the increasing sea state. Undesired flight oscilation becomes significant after sea state 6, and above that, flight performance is basically not acceptable.

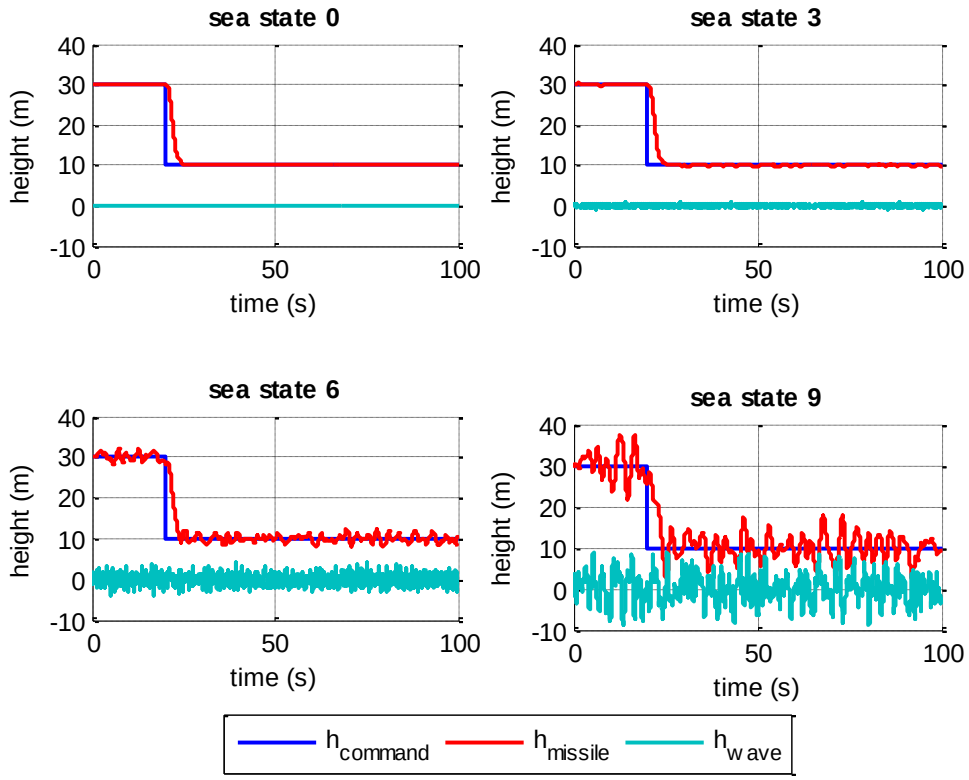

Figure 3.14 : Performance of the Altitude Controller for Different Sea States

In Figure 3.15, performance of the altitude controller is shown for both ideal altimeter and noisy altimeter for sea state 0 and 6. For the sea state 0 case, when altimeter noise is introduced to the system, altitude hold performance degrades such that missile oscillates $\pm 0.5m$ around the desired altitude with a low frequency, which is close to bandwidth of the closed loop height control system. For the case of state 6, sea wave elevations already disturb the system, as also seen in Figure 3.14. When altimeter noise introduced into sea state 6 condition, oscillations increase just a little bit that actually cannot be noticed easily.

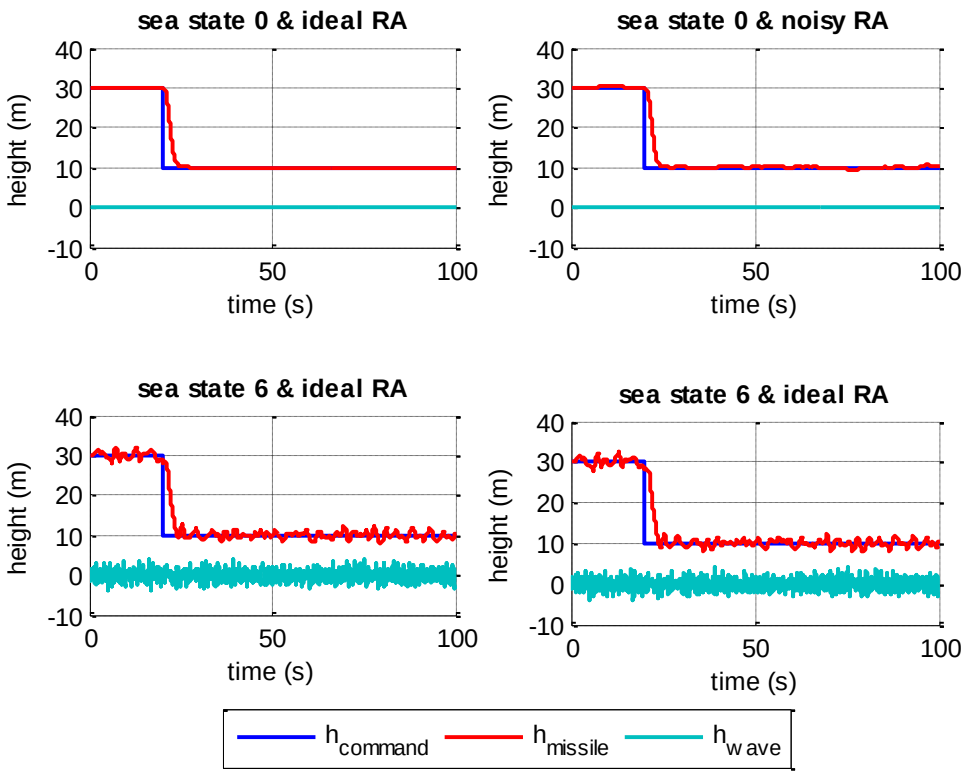

Figure 3.15 : Performance of the Altitude Controller with Radar Altimeter Noise

Note that, IMU feedback is not used in current altitude control system; so, accelerometer bias does not affect the system performance yet since only RA is used for altitude and altitude rate feedback. On the other hand, note also that altitude controller runs in 100 Hz discrete time, which satisfies the condition in part 3.4.3.

From these results, it can be deducted that, for low sea states, altimeter noise is more dominant in the deteriorated system performance, while for high sea states, sea wave elevation itself causes system performance to be poor. In either case, when a missile flying at low altitude especially below 10 meters is considered, following the desired altitude command with $\pm 2\ m$ is unacceptable. Therefore, it is obvious that a robust controller against these disturbances is definitely needed.

CHAPTER 4

ROBUST ALTITUDE CONTROL SYSTEM

4.1 Previous Approaches

Having stated that a robust altitude controller for a sea skimming missile is a necessity, former studies about this specific topic are investigated in this part. As already summarized in literature survey in part 1.2, there are a few studies directly analyzing this particular topic. But for the sake of simplicity, the most two comprehensive studies are examined in detail.

4.1.1 Two-State Kalman Filter Based Controller

In the study [12], linear quadratic regulator (LQR) is used to design the height control system. For the availability of the states and in order to handle sea wave disturbance, following the linear quadratic Gaussian (LQG) structure, KF based controller is designed and performance of the system is analyzed. In this work, both the controller structure and missile configuration are different from those in studies [12] and [13]. Thus, rather than directly using the KF based height controller proposed in [13], a new KF based height control system is designed at this part using the classical height control system presented in part 3.3.

Knowing that plant is given by a double integrator, discrete time system dynamics and measurement equations are written as;

$$\begin{aligned} x_{k+1} &= Ax_k + Bu_k + w_k \\ y_{k+1} &= Cx_k + v_k \end{aligned} \tag{4.1}$$

where w_k and v_k are both white noise vectors being process and measurement noise; respectively. The discrete system matrices are;

$$A = \begin{bmatrix} 1 & dt \\ 0 & 1 \end{bmatrix} \qquad B = \begin{bmatrix} dt^2/2 \\ dt \end{bmatrix} \qquad C = \begin{bmatrix} 1 & 0 \\ 0 & 1 \end{bmatrix}$$
$$x = \begin{bmatrix} h \\ \dot{h} \end{bmatrix} \qquad u = a_m \tag{4.2}$$

Since, there are two radar altimeter measurements, noise level on each measurement is different and will be taken as given in part 3.4.1. In order to obtain noise free measurements, Kalman filter estimates will be used. Discrete time Kalman filter dynamics consist of time update and measurement update equations [35]; which are;

$$\begin{aligned} \hat{x}_{k+1}^- &= A\hat{x}_k + Bu_k \\ P_{k+1}^- &= AP_kA^T + Q \\ K_{k+1} &= P_{k+1}^- C^T (CP_{k+1}^- C^T + R)^{-1} \\ \hat{x}_{k+1}^+ &= \hat{x}_{k+1}^- + K_{k+1}(y_{k+1} - C\hat{x}_{k+1}) \\ P_{k+1}^+ &= P_{k+1}^- - K_{k+1}CP_{k+1}^- \end{aligned} \tag{4.3}$$

Since, the system matrix A does not change with time, covariance matrix P and gain matrix K will be constant matrices. After selecting Q and R matrices, one can obtain the state estimate vector $\hat{x}$. Measurement noise covariance matrix R is chosen according to the measurement noise given in part 3.4.1. On the other hand, process noise covariance matrix, Q to be selected, can be considered as a measure of reliability on either measurements or system model excited by the input. Thus, alternatively, Q matrix can be computed via a q value. As the magnitude of q approaches zero, states are estimated through the system model and Kalman filter ignores the measurements. Setting $q = 0.01$ is a reasonable choice for this system. The resulting R and Q matrices are obtained as in the equation (4.4).

$$\begin{aligned} R &= \begin{bmatrix} \sigma_{h_{RA}}^2 & 0 \\ 0 & \sigma_{\dot{h}_{RA}}^2 \end{bmatrix} = \begin{bmatrix} 1^2 & 0 \\ 0 & 1.5^2 \end{bmatrix} \\ Q &= Bq^2B^T = 0.01^2 \begin{bmatrix} dt^4/4 & dt^3/2 \\ dt^3/2 & dt^2 \end{bmatrix} \end{aligned} \tag{4.4}$$

Now Kalman filter is ready to estimate the height and the height rate, by aiding the radar altimeter measurements with accelerometer measurement. Then, using the

estimated states in the height control loop, rather than measurements directly, algorithm shown in block diagram in Figure 4.1 is obtained.

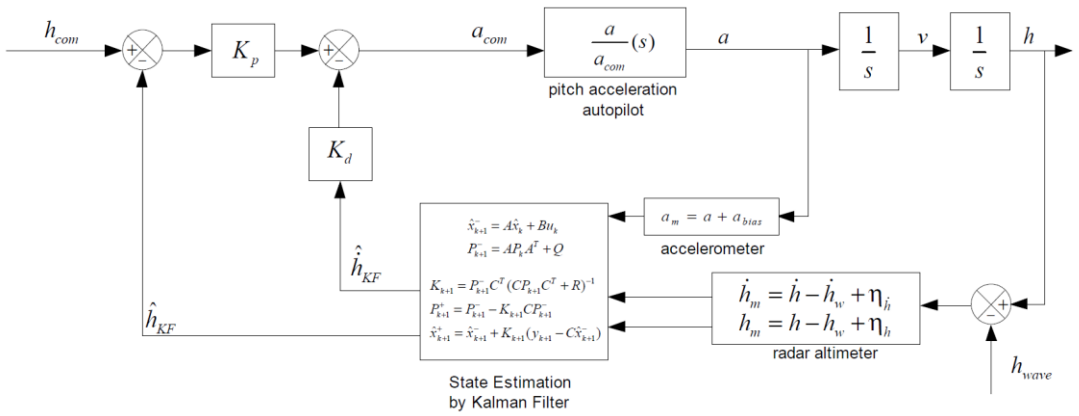

Figure 4.1 : Block Diagram of 2-State Kalman Filter Based Height Controller

4.1.2 Extended State Observer Based Controller

In the study [17], ESO based height control system is proposed to overcome sea wave disturbance problem. ESO is said to be successful in estimating sea wave elevations in real time. Once the wave height is estimated, one can subtract it from altimeter measurements to obtain height above mean sea level. A block diagram for ESO based height control is shown in Figure 4.2.

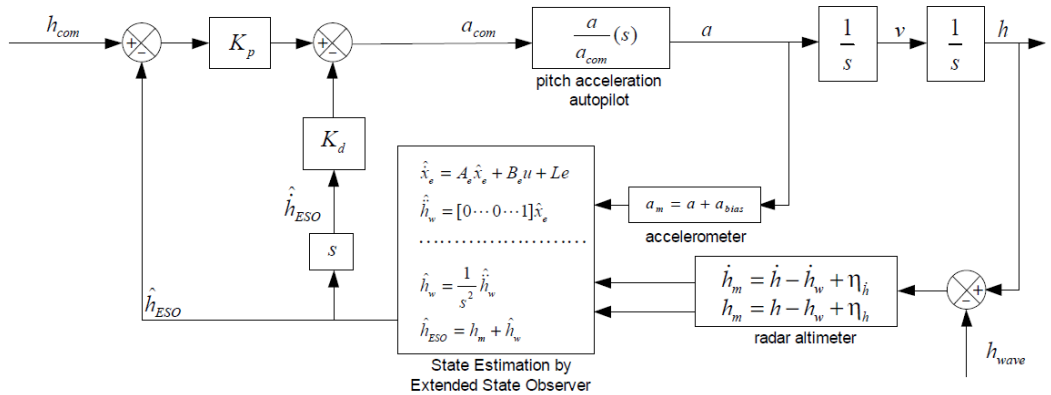

Figure 4.2 : ESO Based Height Control System

Continuous time system dynamics of the ESO are given as;

$$\begin{aligned} \dot{\hat{x}}_e &= A_e\hat{x}_e + B_e u + Le \\ \hat{y} &= C_e\hat{x}_e \end{aligned} \tag{4.5}$$

The system matrices A_e, B_e and C_e and the error state e for the ESO are defined as;

$$A_e = \begin{bmatrix} 0 & 1 & 0 \\ 0 & 0 & 1 \\ 0 & 0 & 0 \end{bmatrix} \qquad B_e = \begin{bmatrix} 0 \\ 1 \\ 0 \end{bmatrix} \qquad C_e = [1 \quad 0 \quad 0]$$
$$e = y - \hat{y} = x_1 - \hat{x}_1 \tag{4.6}$$

Following the procedure explained in [17], and setting the observer pole locations at -2000 as proposed, gain vector L is obtained as in the equation (4.7).

$$L_{2000} = [6 \times 10^3 \quad 1.2 \times 10^7 \quad 8 \times 10^9] \tag{4.7}$$

Although there is nothing wrong in the above calculations theoretically, observer pole locations at-2000 is far from practical applications. In control theory, it is very well known that; a continuous signal consisting of many frequencies with maximum frequency component ω_{max} can be reconstructed completely from the discrete signal only if the sampling frequency ω_s is larger than at least the twice of the maximum frequency ω_{max}. This is known as Nyquist-Shannon sampling theorem and it can mathematically be expressed as in relation (4.8).

$$\omega_s > 2\omega_{max} \tag{4.8}$$

It is also noted in [36] that, even though the requirement for sampling frequency is specified as twice the frequency of the maximum frequency component, it is stated that practical considerations on the stability of the closed-loop system may force to sample at a frequency much higher than the theoretical minimum, frequently 10-20 times higher. Therefore, it can be deducted that, for a maximum frequency component ω_{max} sampling frequency of the digital computer should be chosen at least 10 times of the maximum frequency.

$$\omega_s = 10\omega_{max} \tag{4.9}$$

In the observer design above, pole locations actually refer to $2000\ rad/s$ frequency component. If it is expected from the observer to work smoothly in a digital computer, according to [36] sampling frequency of the computer should be above 3000 Hz as in the relation given in equation (4.10).

$$\begin{aligned} \omega_s &= 10\omega_{max} = 10 \times (2000)\ rad/s \\ \omega_s &\approx 3183\ Hz \end{aligned} \tag{4.10}$$

Obviously, 3000 Hz discrete computation is far from practicality for a missile onboard computer, since neither any sensor can provide new data at this rate, nor the computer is powerful enough to run whole calculations in real time. Considering computer power limitation mentioned in part 3.4.3, the problem should be approached reversely. 100 Hz discrete computation forces the controller to have its maximum frequency component to be bounded. Thus, a realistic pole location for same observer design can be chosen as at $-60\ rad/s$ as in the equation set (4.11).

$$\begin{aligned} &\omega_s = 10\omega_{max} \\ &100 \times 2\pi = 10 \times (\omega_{max}) \\ &\omega_{max} = 20\pi \approx 60\ rad/s \end{aligned} \tag{4.11}$$

Finally, a new gain vector L can be obtained accordingly as in the equation (4.12).

$$L_{60} = [180 \quad 10800 \quad 216000] \tag{4.12}$$

4.2 Three-State Kalman Filter Based Robust Altitude Controller

Both methods in previous part are said to eliminate sea wave disturbances by aiding the altimeter measurements with accelerometer data. But neither of them considers the accelerometer bias. In fact, if the IMU measurements were perfect, there would be no need any other sensor data since the navigation solution would have been unspoiled. Therefore, while combining the data from IMU, accelerometer errors should be considered. Specifically, in this case, accelerometer bias is crucial for this kind of sensor fusion applications.

In the pre-study of this thesis [18], extended Kalman filter based estimation algorithm is anticipated in order to estimate accelerometer bias and obtain true altitude as non-drifted. But since the linear analyses are the concern in this study and state matrices do not change with time, actually there is no need to express the system with extended Kalman filter. Addition of the accelerometer bias as a state to nominal Kalman filter should also work well since the unknown bias to be estimated is also constant with time. By this motivation, re-writing the accelerometer measurement equation (3.22) and position velocity acceleration relation in discrete time at time k, equation set (4.13) is obtained.

$$\begin{aligned} a_k &= a_{m\,k} - a_{bias} \\ v_{k+1} &= v_k + a_{k+1}\,dt \\ v_{k+1} &= v_k + a_{m\,k+1}dt - a_{bias}dt \\ h_{k+1} &= h_k + v_k dt + a_{k+1}\frac{dt^2}{2} \\ h_{k+1} &= h_k + v_k dt + a_{m\,k+1}\frac{dt^2}{2} - a_{bias}\frac{dt^2}{2} \end{aligned} \tag{4.13}$$

Open form of the state-space system can be written as in (4.14)

$$\begin{aligned} \begin{bmatrix} h \\ v \\ a_{bias} \end{bmatrix}_{k+1} &= \begin{bmatrix} 1 & dt & -dt^2/2 \\ 0 & 1 & -dt \\ 0 & 0 & 1 \end{bmatrix} \begin{bmatrix} h \\ v \\ a_{bias} \end{bmatrix}_k + \begin{bmatrix} dt^2/2 \\ dt \\ 0 \end{bmatrix} a_{m\,k+1} \\ \begin{bmatrix} h_m \\ v_m \\ a_m \end{bmatrix}_{k+1} &= \begin{bmatrix} 1 & 0 & 0 \\ 0 & 1 & 0 \\ 0 & 0 & 0 \end{bmatrix} \begin{bmatrix} h \\ v \\ a_{bias} \end{bmatrix}_{k+1} + \begin{bmatrix} 0 \\ 0 \\ 1 \end{bmatrix} a_{m\,k+1} \end{aligned} \tag{4.14}$$

Closed form of the system can be expressed as in (4.15).

$$\begin{aligned} x_{k+1} &= Ax_k + Bu_{k+1} \\ y_{k+1} &= Hx_{k+1} + Du_{k+1} \end{aligned} \tag{4.15}$$

Before writing the Kalman filter equations, note that, there are two slightly different approaches for measurement covariance update as shown in equation (4.16).

$$\begin{aligned} P_{k+1}^{+} &= (I - K_{k+1}H_{k+1})P_{k+1}^{-}(I - K_{k+1}H_{k+1})^T + K_{k+1}R_{k+1}K_{k+1}^T \\ P_{k+1}^{+} &= (I - K_{k+1}H_{k+1})P_{k+1}^{-} \end{aligned} \tag{4.16}$$

Although common choice for Kalman filter equations is the second expression due to its simplicity by means of computation, as also used in the previous height control method, first expression is said to be more stable and robust than the second expression [37]. It is called as the Joseph stabilized version of the covariance measurement update equation and it guarantees that P_{k+1}^{+} will always be symmetric positive definite as long as P_{k+1}^{-} is symmetric positive definite.Second expression, on the other hand, may result with a deteriorated covariance matrix as the time passes within computation steps; which yields to poor estimation of states. Therefore, using Joseph stabilized version of the covariance update equation in this Kalman filter, filter equation set, consisting of time and measurement update equations, is obtained as in (4.17).

$$\begin{aligned}\hat{x}_{k+1}^{-} &= A\hat{x}_k + Bu_{k+1}\\ P_{k+1}^{-} &= AP_kA^T + Q\end{aligned}$$

$$\begin{aligned}K_{k+1} &= P_{k+1}^{-}H^T(HP_{k+1}^{-}H^T + R)^{-1}\\ \hat{x}_{k+1}^{+} &= \hat{x}_{k+1}^{-} + K_{k+1}(y_{k+1} - H\hat{x}_{k+1})\\ P_{k+1}^{+} &= (I - K_{k+1}H)P_{k+1}^{-}(I - K_{k+1}H)^T + K_{k+1}RK_{k+1}^T\end{aligned} \tag{4.17}$$

Once the designer chooses proper Q and R matrices, Kalman filter is ready to estimate state vector $\hat{x}$. R matrix is chosen according to the altimeter noise level and order of the accelerometer bias. On the other hand, Q matrix should be chosen by considering the desired noise level on the estimated states as well as considering the stability issues. For the calculation of Q matrix, $q = 10^{-5}$ seems to work well after trial-error runs. All in all, Kalman filter design is finalized with the selected matrices as in equation (4.18).

$$\begin{aligned}R &= \begin{bmatrix}\sigma_{h_{RA}}^2 & 0 & 0\\ 0 & \sigma_{h_{RA}}^2 & 0\\ 0 & 0 & O(a_{bias})\end{bmatrix} = \begin{bmatrix}1^2 & 0 & 0\\ 0 & 1.5^2 & 0\\ 0 & 0 & 0.01^2\end{bmatrix}\\ Q &= Bq^2B^T = 10^{-10}\begin{bmatrix}dt^4/4 & dt^3/2 & 0\\ dt^3/2 & dt^2 & 0\\ 0 & 0 & 0\end{bmatrix}\end{aligned} \tag{4.18}$$

After finalizing the Kalman filter design by choosing the design parameters, now it is ready to integrate filter into height control system. Kalman filter will work online in the algorithm with the height controller. External input data to the Kalman filter are the altimeter measurements h_m and $\dot{h}_m$ as well as with the accelerometer data a_m. States of the Kalman filter which will be estimated are; height $\hat{h}_{KF}$, vertical velocity $\hat{v}_{KF}$ and accelerometer bias $\hat{a}_{bias}$.

Moreover, after estimating the altitude over mean sea level by Kalman filter, one can also obtain instantaneous wave height estimation by subtracting it from the altimeter height measurement as in equation (4.19). This estimation will be used in determination of the optimum altitude process in CHAPTER 5.

$$\begin{aligned} h_m &= h - h_{wave} + \eta_h \\ \hat{h}_{wave} &= \hat{h}_{KF} - h_m \end{aligned} \tag{4.19}$$

Recall from previous chapter that, noise rejection performance of the default altitude controller was very poor since there are considerable amount of frequency components in wave elevations very close to system bandwidth. Actually it is the reason why a typical low-pass filter cannot be used to solve this problem. The cut of frequency of a low pass filter should be very low to overcome sea wave disturbance but applying such a low cut off frequency would deteriorate the closed loop system. On the other hand, when Kalman filter is integrated with the altitude controller, Figure 3.12 changes significantly and Figure 4.3 is obtained. Firstly, Bode magnitude diagram of command tracking transfer function remains same; which means system performance of the designed closed loop did not change as desired. Secondly and more importantly, Bode magnitude diagram for wave rejection transfer function shifts to the left; which means, there has been an improvement in rejecting noises within considerable range of frequencies.

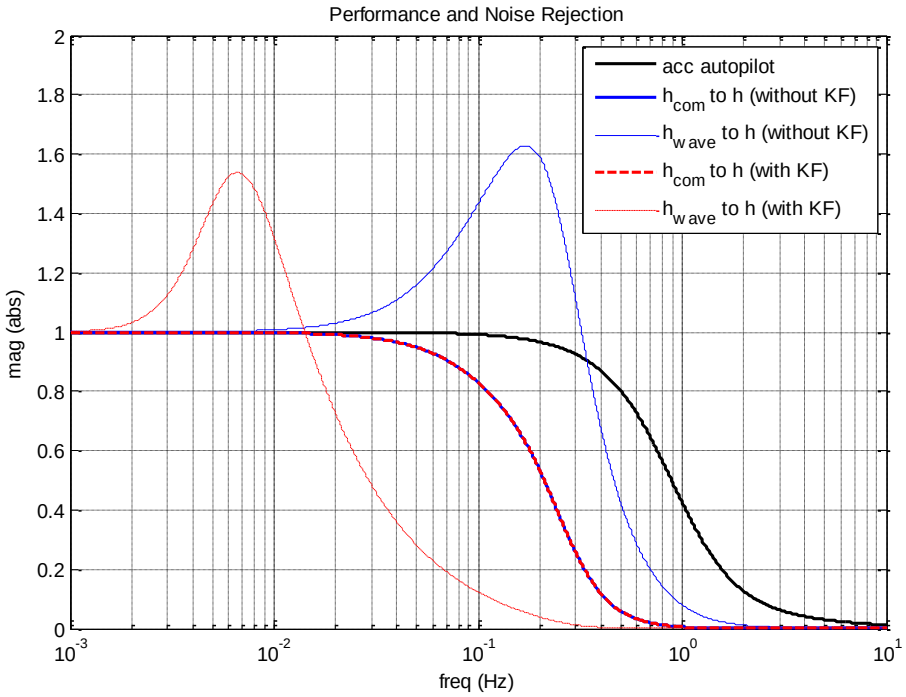

Figure 4.3 : Bode Diagram of the Altitude Controller with and without KF

4.3 Comparative Simulation Results and Discussion

Having designed the different altitude controllers, now they can be compared with each other under several distinct scenarios. Six controllers to be compared will be; classical RA feedback based controller, controller which is using simply INS solution, two-state Kalman filter based controller from 4.1.1, continuous and discrete ESO based controllers from 4.1.2 and three-state Kalman filter based controller in 4.2 which is the proposed method.

Test scenarios for comparison are decided such that; the question, how each individual disturbance or error affects different height control methods has a satisfactory answer. Starting with the ideal case; first, only the altimeter noise will be introduced to system. Then the performance of the controllers will be investigated under the effect of sea waves. After that, accelerometer bias will be considered. And finally, all the disturbances and errors will be considered for simulations.

Performances of the controllers for each distinct condition can be compared by graphical inspection. But actually, it is not enough to come to a deterministic conclusion just by analyzing graphics. Therefore, an analytical method should also be used to determine success of each simulation. Planning the simulations as having the same altitude command profile and duration as in Figure 3.14 and Figure 3.15, a reasonable choice for the analytical method seems to be usage of mean and standard deviation of achieved altitudes. Also in order to neglect transient effects, for the success criteria only the last 50 seconds will be considered. So, let the achieved altitude throughout the simulation to be expressed as $\bar{h}$ array, with a corresponding time array $\bar{t}$ as in equation (4.20).

$$\bar{h} = \begin{bmatrix} h_1 \\ h_2 \\ \vdots \\ h_N \end{bmatrix} \quad ; \quad \bar{t} = \begin{bmatrix} t_1 \\ t_2 \\ \vdots \\ t_N \end{bmatrix} = \begin{bmatrix} \delta t \\ 2\delta t \\ \vdots \\ N\delta t \end{bmatrix} = \begin{bmatrix} 0.01 \\ 0.02 \\ \vdots \\ 100 \end{bmatrix} sec \tag{4.20}$$

Mean achieved altitude μ_h can be calculated with the data of $\bar{h}$ after $t = 50sec$. Moreover, one can obtain the deviation of the mean achieved altitude $\Delta\mu_h$ by subtracting it from the commanded altitude as also seen in equation (4.21).

$$\mu_h \,|_{50<t<100} = \frac{\sum_{i=5000}^{i=10000} h_i}{5000}$$
$$\Delta\mu_h = |h_{com} - \mu_h| \tag{4.21}$$

Similarly, standard deviation of the same data σ_h for the same time interval is calculated as in equation (4.22).

$$\sigma_h \,|_{50<t<100} = \sqrt{\frac{\sum_{i=5000}^{i=10000} (\mu_h - h_i)^2}{5000}} \tag{4.22}$$

4.3.1 Simulation Results for Ideal Case

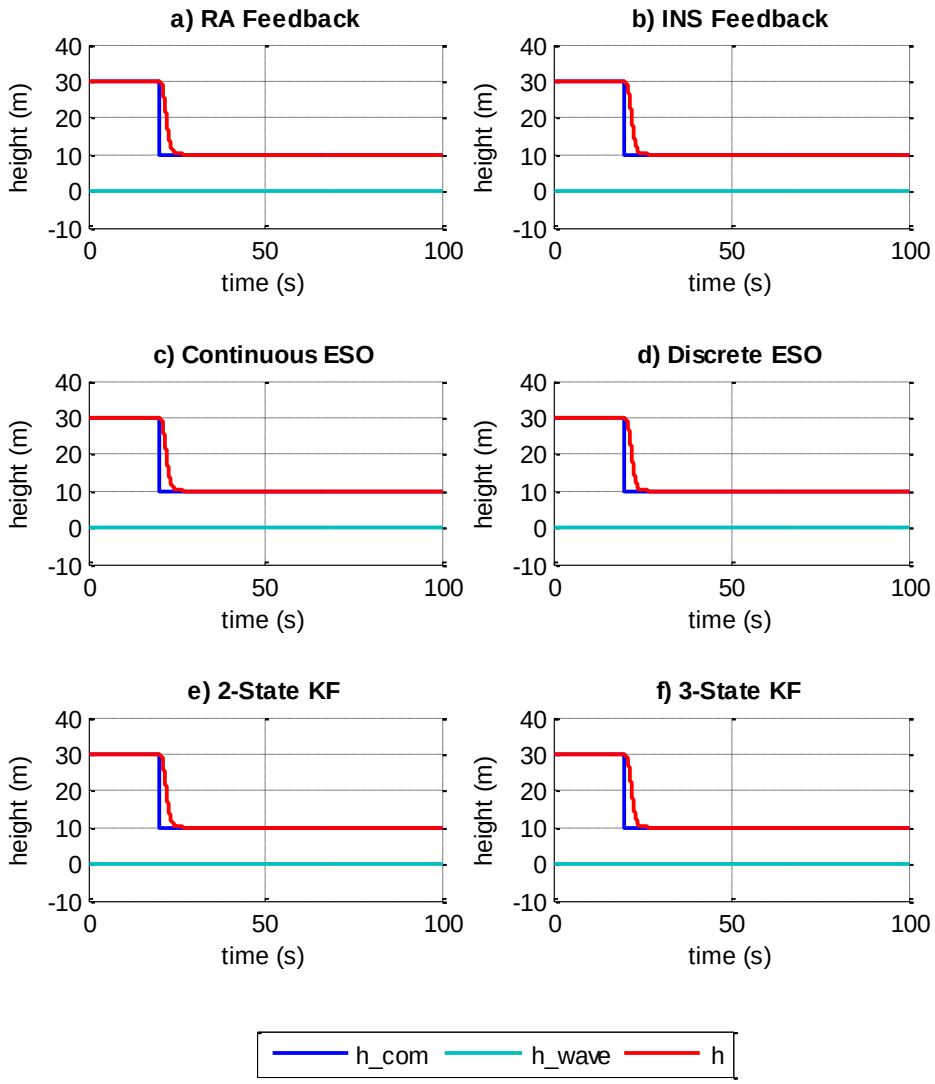

Figure 4.4 : Graphical Comparison of Height Controllers for Ideal Case

Table 4.1 : Analytical Comparison of Height Controllers for Ideal Case

	$\Delta\mu_h \mid_{50<t<100}$ $[m]$	$\sigma_h \mid_{50<t<100}$ $[m]$
RA Feedback	0.00	0.0000
INS Feedback	0.00	0.0000
Continuous ESO	0.00	0.0000
Discrete ESO	0.00	0.0000
2-State KF	0.00	0.0000
3-State KF	0.00	0.0000

4.3.2 Simulation Results for Radar Altimeter Noise Case

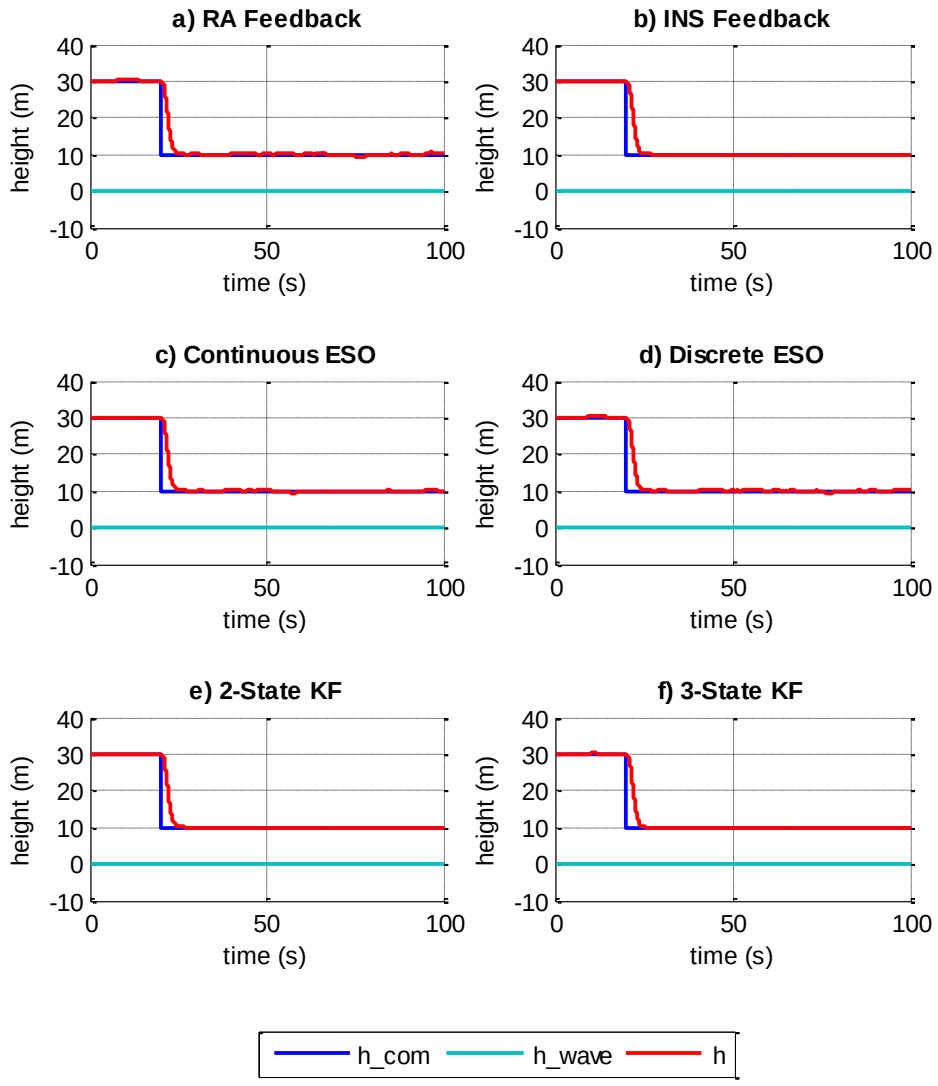

Figure 4.5 : Graphical Comparison of Height Controllers for RA Noise Case

Table 4.2 : Analytical Comparison of Height Controllers for RA Noise Case

	$\Delta\mu_h \mid_{50<t<100}$ $[m]$	$\sigma_h \mid_{50<t<100}$ $[m]$
RA Feedback	0.04	0.2870
INS Feedback	0.00	0.0000
Continuous ESO	0.05	0.1505
Discrete ESO	0.03	0.2431
2-State KF	0.01	0.0534
3-State KF	0.00	0.0529

4.3.3 Simulation Results for Sea Wave Disturbance Case

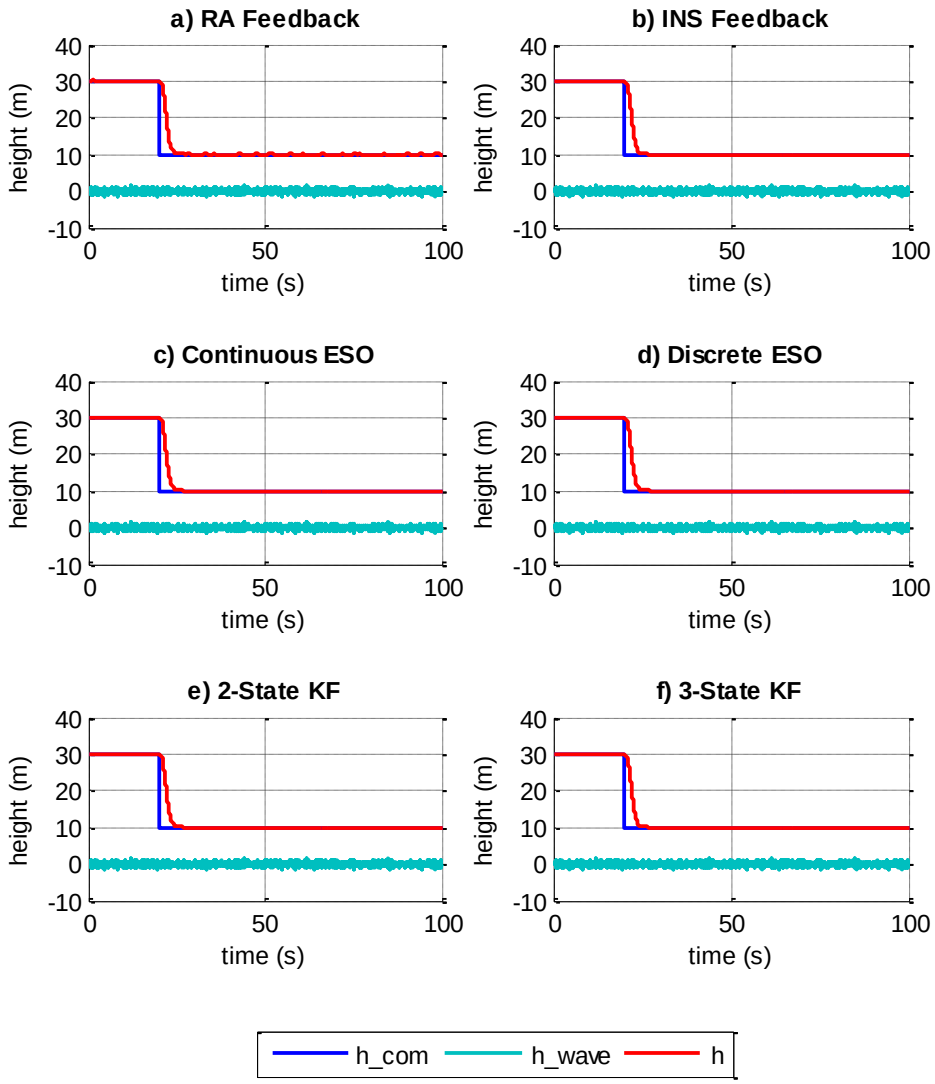

Figure 4.6 : Graphical Comparison of Height Controllers for Sea State 4 Case

Table 4.3 : Analytical Comparison of Height Controllers for Sea State 4 Case

	$\Delta\mu_h \mid_{50<t<100}$ $[m]$	$\sigma_h \mid_{50<t<100}$ $[m]$
RA Feedback	0.00	0.0609
INS Feedback	0.00	0.0017
Continuous ESO	0.00	0.0018
Discrete ESO	0.01	0.0074
2-State KF	0.00	0.0066
3-State KF	0.00	0.0057

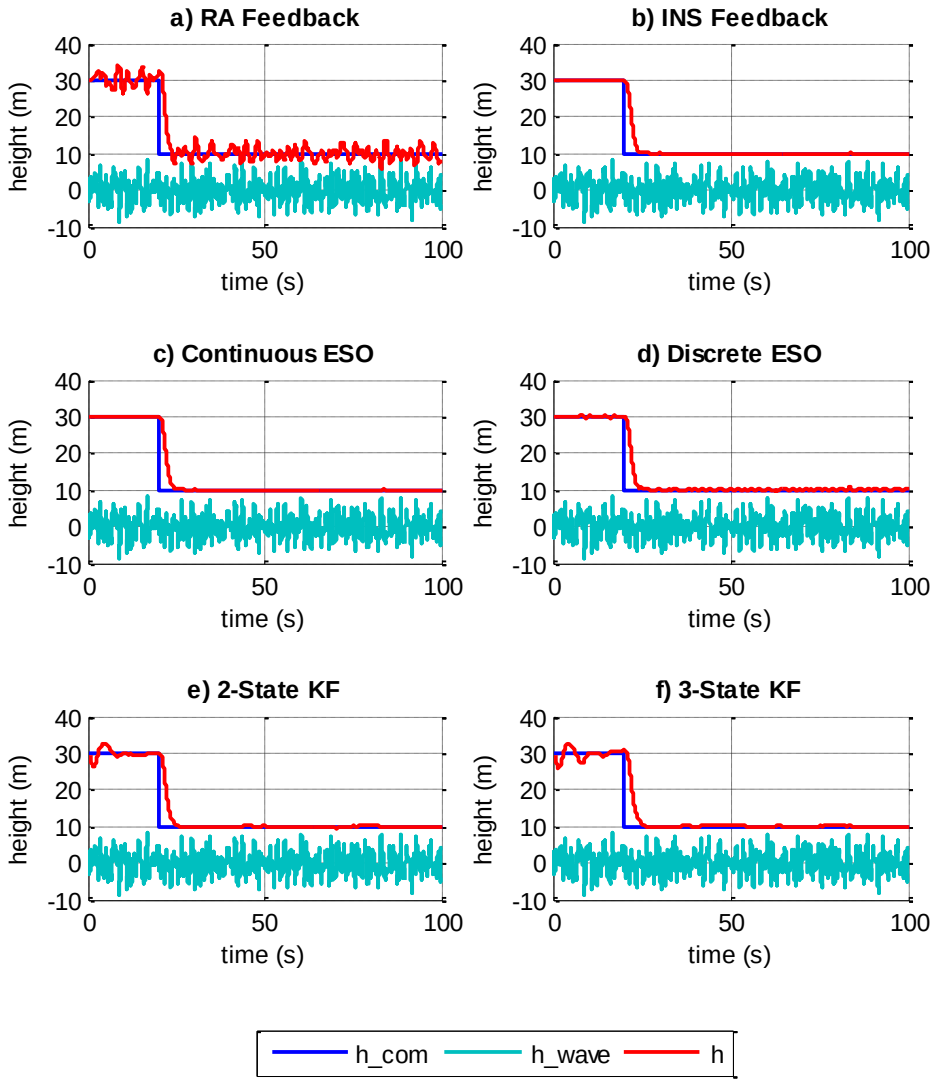

Figure 4.7 : Graphical Comparison of Height Controllers for Sea State 8 Case

Table 4.4 : Analytical Comparison of Height Controllers for Sea State 8 Case

	$\Delta\mu_h \mid_{50<t<100}$ $[m]$	$\sigma_h \mid_{50<t<100}$ $[m]$
RA Feedback	0.09	1.6345
INS Feedback	0.00	0.0412
Continuous ESO	0.00	0.0438
Discrete ESO	0.14	0.1745
2-State KF	0.08	0.1670
3-State KF	0.02	0.1424

4.3.4 Simulation Results for Accelerometer Bias Case

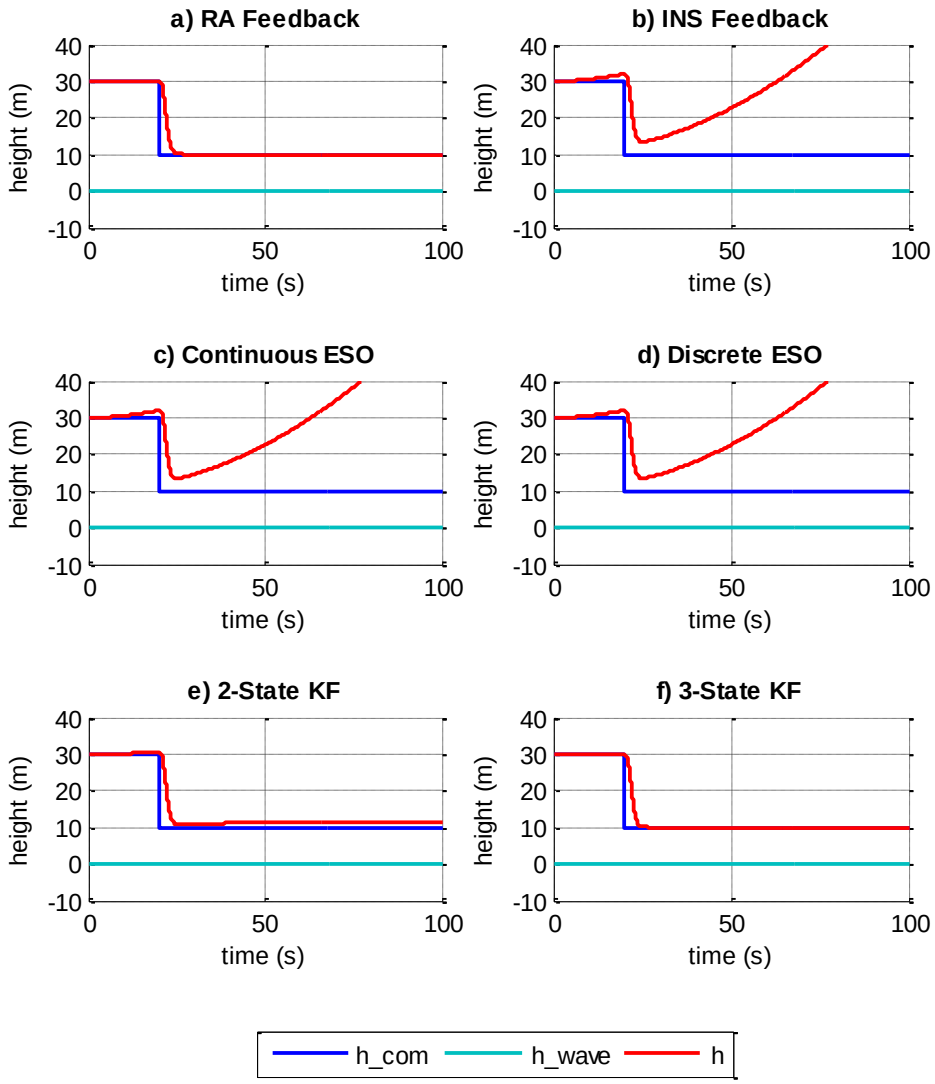

Figure 4.8 : Graphical Comparison of Height Controllers for IMU Bias Case

Table 4.5 : Analytical Comparison of Height Controllers for IMU Bias Case

	$\Delta\mu_h \mid_{50<t<100}$ $[m]$	$\sigma_h \mid_{50<t<100}$ $[m]$
RA Feedback	0.00	0.0000
INS Feedback	29.15	10.8681
Continuous ESO	29.14	10.8679
Discrete ESO	29.11	10.8616
2-State KF	1.24	0.0274
3-State KF	0.00	0.0012

4.3.5 Simulation Results for All Disturbances and Errors Included

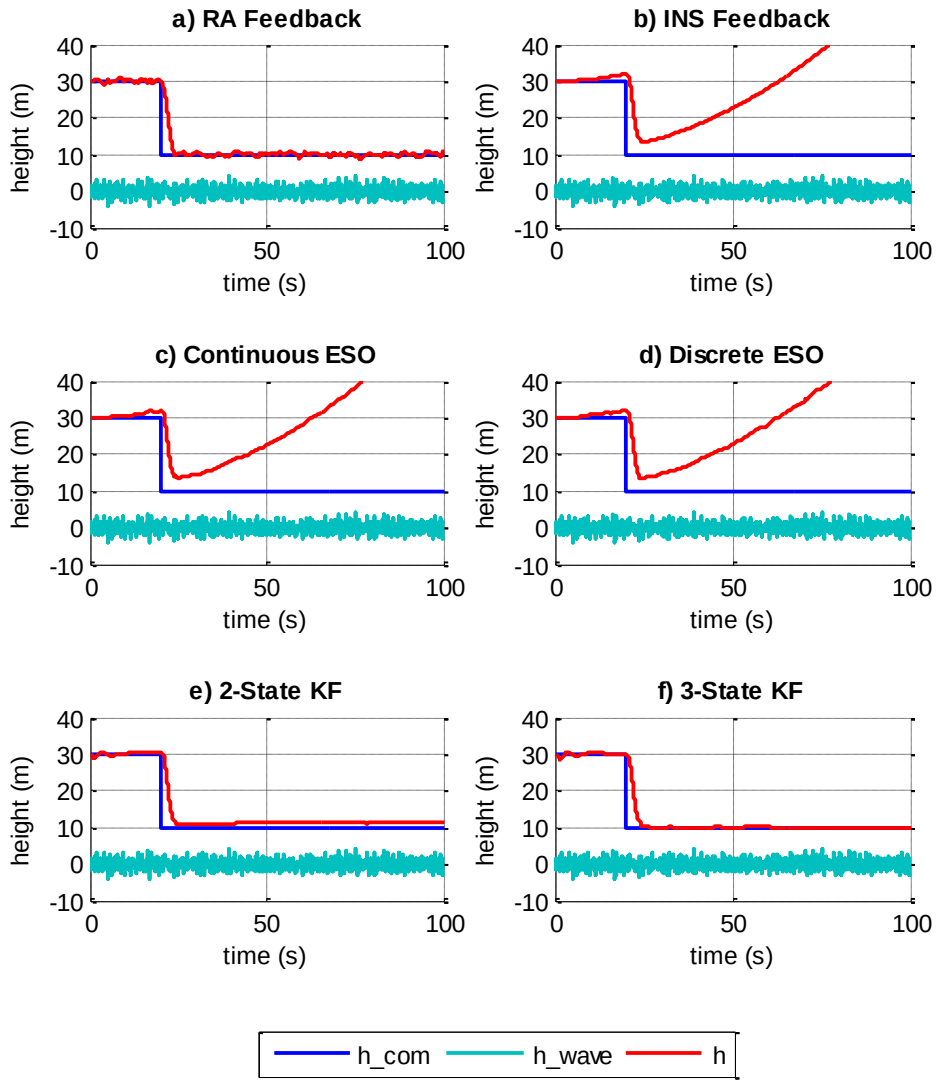

Figure 4.9 : Graphical Comparison of Height Controllers with All Effects

Table 4.6 : Analytical Comparison of Height Controllers with All Effects

	$\Delta\mu_h \mid_{50<t<100}$ $[m]$	$\sigma_h \mid_{50<t<100}$ $[m]$
RA Feedback	0.03	0.4689
INS Feedback	29.15	10.8680
Continuous ESO	29.19	10.9614
Discrete ESO	29.20	10.8770
2-State KF	1.24	0.0717
3-State KF	0.03	0.0557

4.3.6 Discussion

For the ideal case, as expected, all the results for each height control method are just perfect as can be seen from Figure 4.4 and Table 4.1. Neither the mean achieved altitude deviates from the commanded altitude, nor an oscillation is observed since there is no disturbance or error or uncertainty in the systems.

Introducing the radar altimeter noise to the system, slight degradations in the command tracking performance is observed as seen in Figure 4.5 and Table 4.2. Only the performance of the controller with IMU feedback remains same since RA measurements are not used in that control loop. Apart from that, 3-state KF based controller is the most successful one by means of rejecting altimeter noise as can be seen from Table 4.2.

When sea wave disturbances are introduced to the system for sea state 4 condition, by means of both sea wave elevations and gust disturbance due to sustained wind, results in Figure 4.6 and Table 4.3 are obtained. In Figure 4.6 c), d), e) and f), sea wave effects on altitude hold performances are negligible, since all four methods are developed mainly against sea wave disturbance problem.

If sea condition is worsened, say sea state 8 which actually corresponds to very strong wind condition, degradation of the command tracking performance of the controllers becomes considerable. From Figure 4.7 a) RA based controller has the worst altitude hold performance among others. Figure 4.7 b) indicates that INS based controller has still nearly perfect performance since only the gust disturbance is effective on that control loop. From Table 4.4, continuous time ESO based controller performs the best since observer poles are extremely fast. Discrete time ESO based controller, the one actually which is practically implementable, is not as good as the former. On the other hand, performances of both KF based controller are acceptable.

While keeping the other feedbacks perfect, introducing only accelerometer bias error to the systems resulted in interesting consequences on the controllers as seen from Figure 4.8 and Table 4.5. Obviously, performance of the RA based controller did not

change since it does not use any of the accelerometer data. Firstly, as very well known, navigation solution drifts with the bias and INS based controller adopts itself to the drifted navigation solution and diverges. Secondly, same phenomenon occurs for ESO based controllers. They fail since they integrate accelerometer data directly to aid altimeter measurements. 2-state KF based controller tracks the altitude command with a bias which actually changes with the KF design parameter q. While q gets smaller and smaller, KF trusts the mathematical system model rather than the altimeter measurements which makes this bias gets larger. If q is selected too big in order not to come up with a biased altitude track, then KF relies on altimeter measurements much more and noise-rejection performance gets worse. So, in 2-state KF there is a trade-off between trusting the accelerometer or altimeter measurements. On the other hand, 3-state KF based controller performs just well since it estimates the accelerometer bias and eliminates its effect on the system. Thus, 3-state KF based controller becomes prominent among the other controllers.

And lastly, even though the results of previous scenario tell everything, for the sake of completeness, all the disturbances and errors are included in the system at once, with a sea condition of sea state 6. Obviously, 3-state KF based altitude control method has the best performance by means of altitude holding.

All these results show that, among the others, proposed method 3-state KF based height control approach has the only acceptable performance which is actually very good. By rejecting sea wave elevations and altimeter noise, as well as estimating the accelerometer bias, and also running in a discrete digital computer with a limited sampling frequency, 3-state KF based controller provides robustness against many real world effects.

CHAPTER 5

OPTIMAL ALTITUDE PROFILE

Importance of the sea skimming guidance strategy for an anti-ship missile is already pointed out in previous chapters. Relation between missile altitude and the distance at which target radar can detect incoming thread, can simply be calculated as follows.

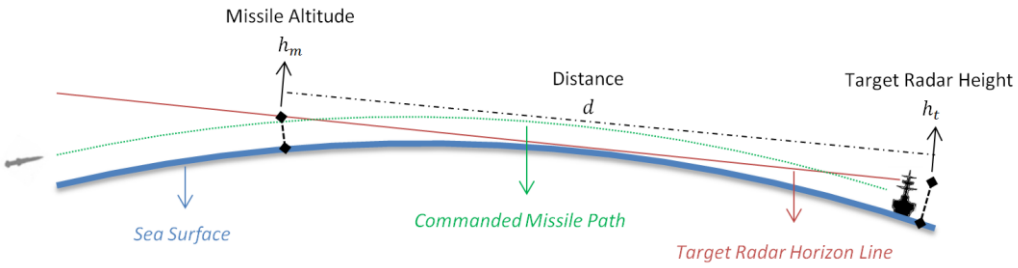

Figure 5.1 : Missile-Target Engagement Geometry

Considering the engagement geometry in Figure 5.1, remaining distance can simply be calculated as in equation (5.1). Here, R_e is the earth radius and for this calculation, earth surface is assumed as to be in circular shape with radius $6378137\ m$.

$$d = \sqrt{2R_e h_m + h_m^2} + \sqrt{2R_e h_t + h_t^2} \tag{5.1}$$

Remaining distance can also be thought as remaining time to hit since velocity of the missile is nearly constant. Subjected missile in this study is cruising at the speed of 0.8 Mach, which is approximately $272\ m/s$. Then, time-to-go is calculated as in equation (5.2).

$$t_{2go} = \frac{d}{V} \approx \frac{d}{272} \tag{5.2}$$

Assuming the target radar to be at 10m above mean sea level, remaining distance and time to go for different missile altitudes are tabulated in Table 5.1 for the time when targeted ship captures the incoming thread. But note that both these distances and durations are theoretical values. In real world, there will be different phenomenon like sea wave clutter, atmospheric disturbance and etc. which at the end shortens the remaining time to hit values even more.

Table 5.1 : Relation between Missile Altitude and Remaining Distance & Time

$h_{missile}\ [m]$	$\sim d\ [km]$	$\sim t_{2go}\ [s]$
0	11.3	42
5	19.3	71
10	22.6	83
15	25.1	92
20	27.3	100
30	30.9	113
50	36.5	134

As clearly seen, remaining time to hit is very different for each missile altitude for the radar of the target ship. For example, flying at a 5m altitude rather than 15m provides missile an extra 20 seconds before detection occurs, which is a huge advantage.

Recall that from Table 2.1, sea wave elevations differ from perfect straight sea surface to waves having above 10m height. So, at which altitude should the missile be flown is a critical problem for the controller designer. One may choose a safe altitude which covers whole sea states and disturbances. But the drawback of this easy method becomes early detection by target ship. On the other hand, commanding an altitude according to different sea states is possible, if sea state is known or calculated somehow at each instant.

In this chapter, first sea waves are analyzed statistically, and then a method is proposed to produce an optimal flight altitude during flight. Procedure of obtaining this optimal altitude is explained in detail.

5.1 Statistical Analyses of Wave Height

Instantaneous wave height seen by the radar altimeter as missile flying forward with 0.8 Mach speed, is needed to be analyzed. When wave model output for a certain time interval is analyzed by distribution of wave elevations for different sea states, histograms in Figure 5.2 are obtained. Shape of the histogram comes out to be very familiar, known as Gaussian distribution with zero mean. Then one can also obtain standard deviations and get the analytical probability density function (PDF) curve.

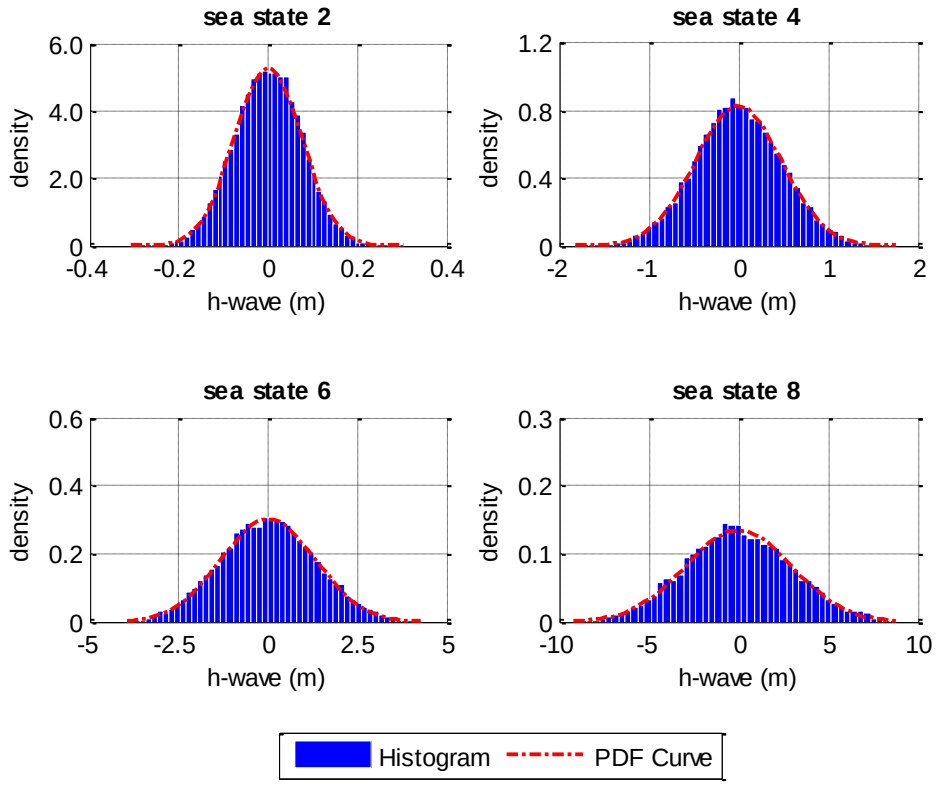

Figure 5.2 : Histogram of Wave Data and PDF Curves for Different Sea States

Related standard deviation values calculated from wave data is shown in Table 5.2.

Table 5.2 : Standard Deviation of Wave Elevations for Sea States

sea state	***standard deviation σ [m]***
2	0.0754
4	0.4812
6	1.3189
8	2.9631

Gaussian distribution, also known as normal distribution, can be defined as a two-parameter family of curves. The first parameter μ is the mean. The second parameter σ is the standard deviation. A general PDF of the normal distribution is defined as in equation (5.3). Note that sea waves occur with zero mean and the curves in Figure 5.2 are plotted with zero mean PDF formula in equation (5.3).

$$PDF = \frac{1}{\sqrt{2\sigma^2\pi}}\, e^{-\frac{(x-\mu)^2}{2\sigma^2}} \quad ; \quad PDF_{\mu=0} = \frac{1}{\sqrt{2\sigma^2\pi}}\, e^{-\frac{x^2}{2\sigma^2}} \tag{5.3}$$

Cumulative distribution function (CDF) of the normal distribution is formulated as in equation (5.4). One can calculate the probability of wave height being smaller than a certain threshold by using CDF.

$$CDF = \frac{1}{2}\left(1 + \text{erf}\left(\frac{x-\mu}{\sigma\sqrt{2}}\right)\right) \quad ; \quad CDF_{\mu=0} = \frac{1}{2}\left(1 + \text{erf}\left(\frac{x}{\sigma\sqrt{2}}\right)\right) \tag{5.4}$$

CDF curves for different sea states can be seen in Figure 5.3.

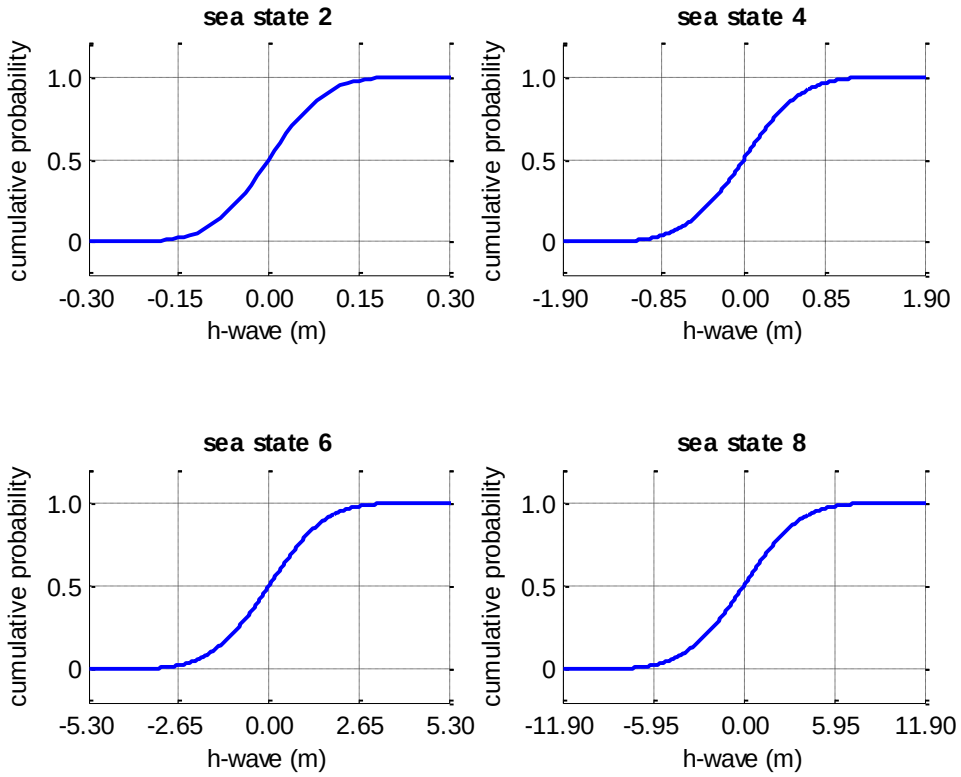

Figure 5.3 : CDF Curves for Different Sea States

Inverse of the CDF is called as quantile and formulated as in equation (5.5). Quantile gives the maximum value of a variable that may have for a certain probability. Thus, one also can calculate the maximum expected wave height for a chosen probability by this formula.

$$Q = \mu + \sigma\sqrt{2}\,\mathrm{erf}^{-1}(2P-1) \quad ; \quad Q_{\mu=0} = \sigma\sqrt{2}\,\mathrm{erf}^{-1}(2P-1) \tag{5.5}$$

Note that both CDF formula in equation (5.4) and quantile equation in (5.5) involve error function erf and its inverse erf^{-1}. These functions do not have an analytical solution but can be solved by numerical methods. More information about error function is provided in APPENDIX C. A table of values for some certain cumulative probabilities and corresponding standard deviation multipliers can be obtained after these equations are solved. In order to make the table independent of the sea state, variable thresholds are kept as multiples of standard deviation and Table 5.3 is obtained. In fact, this is a generalized table valid for any normally distributed data with zero mean, i.e. $\mu = 0$.

Table 5.3 : Normal Distribution Table

$\boldsymbol{std.dev.multiplier}$ $\boldsymbol{K}$	$\boldsymbol{probability}$ $\boldsymbol{P(-K\sigma < x < K\sigma)}$	$\boldsymbol{probability}$ $\boldsymbol{P(x < K\sigma)}$
0.0000	0.0000	**0.5000**
0.2533	0.2000	**0.6000**
0.5244	0.4000	**0.7000**
0.8416	0.6000	**0.8000**
1.0000	0.6827	0.8413
1.2816	0.8000	**0.9000**
1.6449	0.9000	**0.9500**
2.0000	0.9545	0.9772
2.3263	*0.9800*	***0.9900***
3.0000	0.9973	0.9987
3.5000	0.9995	0.9998

For example, if 99% of wave height distribution is desired to be covered, which is highlighted in Table 5.3, threshold is automatically defined as $2.3263 \times \sigma$. This means that risk of encountering a wave height among a certain data set which is larger than the defined threshold is forced to be one percent.

In Figure 5.4, wave elevations for different sea states with the previously mentioned threshold line which corresponds to 1% risk for a certain time interval, are shown.

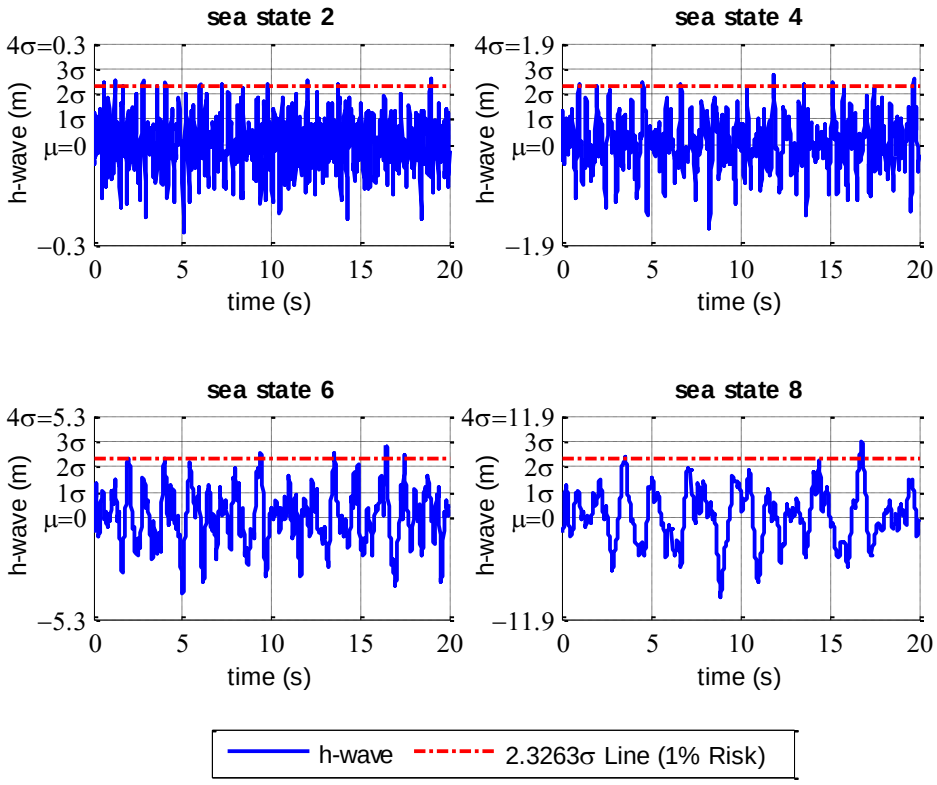

Figure 5.4 : Sea Wave Elevations and 1% Risk Threshold Line

5.2 Determination of the Optimal Flight Altitude

Having analyzed the statistics of sea wave elevations, a proper procedure for determining the optimal flight altitude should be constructed. This altitude should be robust to all the expected disturbances and errors, yet as low as it can be. Moreover, when the long flight of the missile is considered, in which missile travels hundreds of kilometers, this altitude should continuously be adapted according to the flight conditions involved.

First of all, note that instantaneous sea wave elevations are not truly known by the missile computer; hence an estimate for this data is needed. This estimate is already been obtained in CHAPTER 4 and is re-written in equation (5.6).

$$\hat{h}_w = \hat{h}_{KF} - h_m \tag{5.6}$$

In general terms, procedure is built as follows. First, while flying at a higher and a safer altitude, wave estimation data will be collected for a pre-determined time interval. Then, statistical analyses will be performed through the estimated wave data. After that, according to the desired range for a next altitude command to be applied, with an acceptable risk through calculations, an altitude command will be generated. Detailed mathematical expression of this procedure is built step by step as follows.

1) Collect the wave estimation data $\hat{h}_w$ at each time through a pre-determined time interval $T_{sw\#1}$ seconds with a sampling frequency of $100Hz$ $(dt = 0.01s)$ as of the missile computer and obtain the estimated data array $\hat{H}_w$.

$$\begin{aligned} &\hat{H}_w = \left[\hat{h}_w|_{@t_s} \quad \hat{h}_w|_{@t_s+dt} \quad \hat{h}_w|_{@t_s+2dt} \quad \cdots \quad \hat{h}_w|_{@t_s+(N-1)dt}\right] \\ &t_s = time\ at\ which\ data\ collection\ starts \\ &T_{sw\#1} = \ period\ of\ the\ sliding\ window\ \#1 \\ &N = T_{sw} \times 100 = data\ length\ of\ sliding\ window\ \#1 \\ &\hat{H}_w : \ collected\ estimated\ data\ (N\ element\ array) \end{aligned} \tag{5.7}$$

2) At time $t = t_s + Ndt$, having the previous wave estimation data array $\hat{H}_w$, calculate the standard deviation of the wave height distribution by assuming mean wave elevation is zero.

$$\sigma_w = \sqrt{\frac{\Sigma_{k=0}^{k=N}\left(\hat{h}_w|_{@t_s+kdt}\right)^2}{N}} \tag{5.8}$$

3) From the estimated data also calculate the characteristic wave length λ_w by counting the zero-crossings z_w of the wave estimation data array with the assumption of missile is flying with an average velocity of $\bar{V}$ through time interval $T_{sw\#1}$.

$$\lambda_w = \frac{2\,\bar{V}\,T_{sw\#1}}{z_w} \tag{5.9}$$

4) Then define an acceptable risk of R for a single period wave. In order to correlate the optimal altitude to be calculated with the distance or time to be flown, define the probability P by taking into account how many periods of waves with wave length λ_w will be passed during a distance L within a time interval $T_{sw\#2}$, which is the period of the sliding window #2.

$$P = 1 - \frac{R}{L/\lambda_w} = 1 - \frac{R}{(\bar{V}T_{sw\#2}/\lambda_w)} \tag{5.10}$$

5) After that, obtain the standard deviation multiplier K from the new probability with the normal distribution quantile equation.

$$K = \sqrt{2}\,\mathrm{erf}^{-1}(2P - 1) \tag{5.11}$$

6) Finally, achieve a wave-safe altitude which is inside the boundaries of the taken risk by multiplying the calculated factor K with the standard deviation σ.

$$H_{wave-safe} = K\sigma_w \tag{5.12}$$

7) Although a wave-safe altitude is obtained, tracking of the altitude command is never perfect in practice; hence deviation of the missile altitude from commanded altitude σ_h should also be considered and safe altitude is obtained.

$$H_{safe} = K\sqrt{\sigma_w^2 + \sigma_h^2} \tag{5.13}$$

8) And lastly, altimeters working with radio signals encounter a sea clutter in very short distances; which results with invalid measurements. Hence, a bias should also be added in order not to experience a blind range altimeter measurement. All in all, optimal altitude command is formulated as follows.

$$H_{optimal} = RA_{bias} + K\sqrt{\sigma_w^2 + \sigma_h^2} \tag{5.14}$$

5.3 Simulation Results for Different Conditions and Design Parameters

If one would like to obtain a single equation by simplifying the procedure of calculation of the optimal flight altitude in previous part, equation (5.15) is achieved.

$$h_{opt-com} = RA_{bias} + \left[\sqrt{2}\,\mathrm{erf}^{-1}\left(1 - \frac{4RT_{sw\#1}}{z_w T_{sw\#2}}\right)\right]\sqrt{\sigma_w^2 + \sigma_h^2} \qquad (5.15)$$

Variables in equation (5.15) are tabulated in Table 5.4 with their explanation and how they are approached. Altimeter bias is taken as 2m constant value for the design. Deviation of the missile altitude around commanded altitude actually changes according to the sea state, but it can also be taken as constant considering a worst-case scenario. From the analyses in CHAPTER 4, it is already seen that RMS track error does not exceed 0.15m; but still, considering unforeseen disturbances and effects, even a safer value is chosen as 0.30m. For the risk value, 1% seems fine. Taking a high risk may result in wave hit to the missile; while taking the risk value very low causes the optimal altitude determination algorithm be useless.

Table 5.4 : Variables in the Optimal Altitude Calculation Equation

Parameter in equation	Explanation	Usage
$\boldsymbol{RA_{bias}}$ $[\boldsymbol{m}]$	bias for radar altimeter blind range	constant {2m}
$\boldsymbol{\sigma_h}$ $[\boldsymbol{m}]$	deviation of the missile altitude around the commanded altitude	constant {0.3m}
$\boldsymbol{\sigma_w}$ $[\boldsymbol{m}]$	deviation of the estimated wave data $\widehat{H}_w$ around mean sea level along time interval $T_{sw\#1}$	calculated online
$\boldsymbol{z_w}$ $[-]$	zero-crossings of the estimated wave data $\widehat{H}_w$ along time interval $T_{sw\#1}$	calculated online
$\boldsymbol{R}$ [%]	acceptable risk to be chosen	design parameter {1%}
$\boldsymbol{T_{sw\#1}}$ $[\boldsymbol{s}]$	period of sliding window #1 data collection period for statistical analyses	design parameter {10s}
$\boldsymbol{T_{sw\#2}}$ $[\boldsymbol{s}]$	period of sliding window #2 altitude command change period	design parameter {20s , 50s}

Periods of the sliding windows are actually the main design parameters of this algorithm. First window is used for data collection. Estimated wave data is collected along 1st sliding window and statistical analyses are performed at the end of this window. From the analyses, an optimal altitude is obtained and commanded to the altitude controller. At that exact time step, 2nd sliding window starts and holds the optimal altitude command along its period. For the 1st window, duration should not be too long in order to process most up-to-date data more; but, long enough to acquire statistics of wave data. For this period, 10s of time interval seems fine. On the other hand, 2nd window duration may be a little bit longer since frequent altitude command changes are not desired. But, probability of major sea state change along the interval should definitely be considered since it may cause a fatal problem. For this period, two different values; which are 20s and 50s, are applied and output of the simulations is shared in Figure 5.5 for sea state 9 as the worst-case sea condition. As expected, 50s period for $T_{sw\#2}$ case resulted in a bit safer altitude.

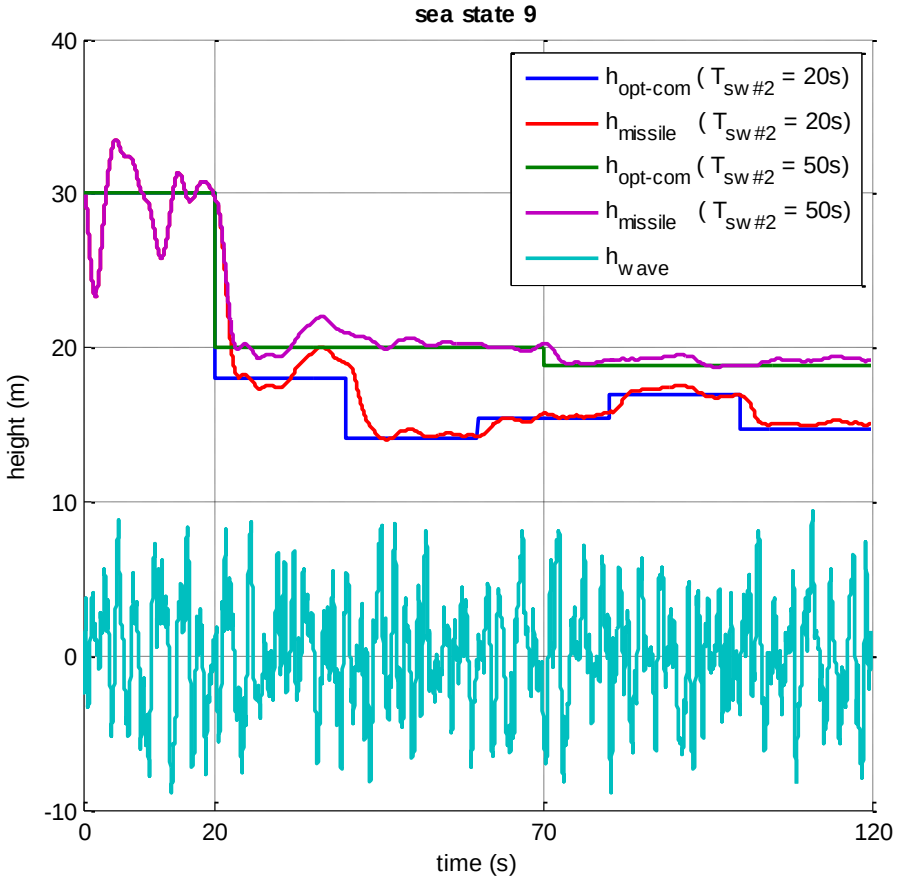

Figure 5.5 : Optimal Altitude Command & Tracking with Different $T_{sw\#2}$ Periods

There is no huge difference between two different periods for $T_{sw\#2}$; thus, larger period is chosen in order to sustain constant altitude for longer time. Timeline of the generation of the optimal altitude command sequence is summarized in Table 5.5.

Table 5.5 : Timeline of Optimal Altitude Command

$0 < t \leq 20$	Initial flight at a safe altitude; $h_{opt-com} = 30$	**$T_{sw\#1}$**	
		$10 \leq t < 20$	Collect $\widehat{H}_{wave}$
		$t = 20$	Calculate $h_{opt-com}$
$T_{sw\#2}$ $20 < t \leq 70$	Fly at $h_{opt-com}$ from previous **$T_{sw\#1}$**	**$T_{sw\#1}$**	
		$60 \leq t < 70$	Collect $\widehat{H}_{wave}$
		$t = 70$	Calculate $h_{opt-com}$
$T_{sw\#2}$ $70 < t \leq 120$	Fly at $h_{opt-com}$ from previous **$T_{sw\#1}$**	**$T_{sw\#1}$**	
		$110 \leq t < 120$	Collect $\widehat{H}_{wave}$
		$t = 120$	Calculate $h_{opt-com}$
⋮	⋮	⋮	⋮

For the sake of completeness, results for some other sea states are shown all in once in Figure 5.6 with $T_{sw\#2}$ 50s.

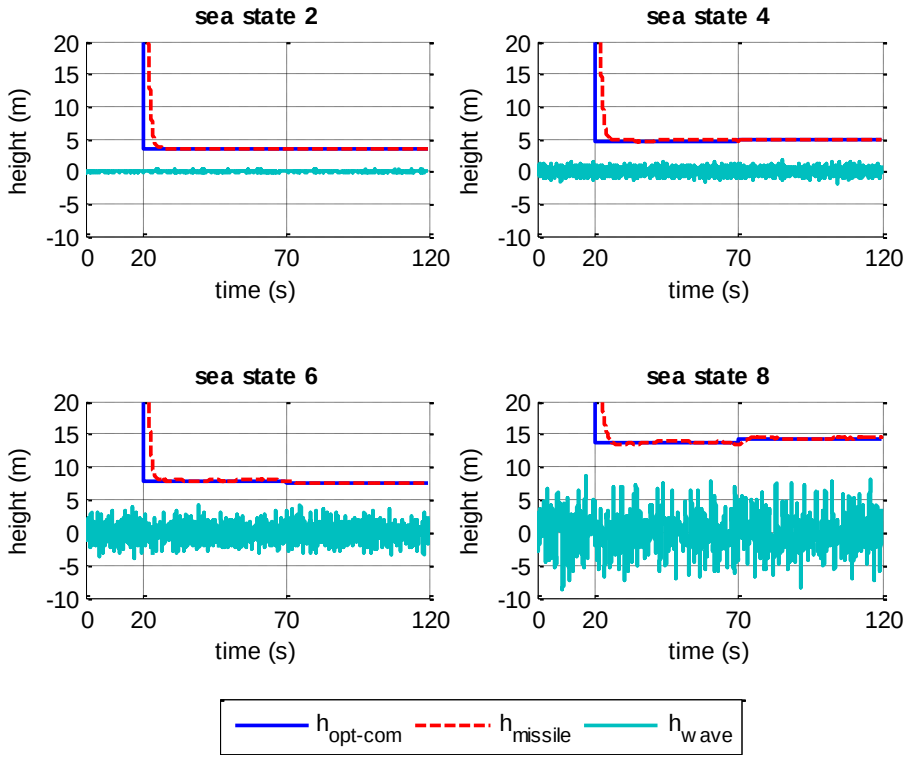

Figure 5.6 : Optimal Altitude Command & Tracking for Different Sea States

Note that, throughout each separate simulation above, sea state remained constant. In fact, effectiveness of the optimal altitude determination algorithm can better be observed for a varying sea condition. For this purpose, two other simulation conditions should be created. First, decreasing sea state condition will be considered and adaptation of the altitude command will be analyzed. Secondly and more importantly, increasing sea state condition will be deliberated and reaction of the missile will be explored. For the variation of sea condition during a single simulation; obviously, sea state change should be adjusted within physical constraints. In real world, sea condition does not alter within small distances and in short time intervals. Yet, for an easy construction and a clear observation, sea state change period will be modeled as 50 seconds, even if it corresponds to a much more harsh change than the real world reflection. Table 5.6 shows the scenarios of two different varying sea state simulation condition.

Table 5.6 : Time Table for Sea State Variation Scenarios

	$t \leq 50$	**$50 < t \leq 100$**	**…**	**$300 < t \leq 350$**	**$350 < t$**
case #1 decreasing sea state	sea state 8	sea state 7	…	sea state 2	sea state 1
case #2 increasing sea state	sea state 1	sea state 2	…	sea state 7	sea state 8

Figure 5.7 shows the simulation result for decreasing sea state case. It is observed that the optimal command generation algorithm performs well by means of adapting to the sea condition. Similarly, in Figure 5.8 simulation result for increasing sea state case is seen. In fact, sea state change from 1 to 8 in 400-second time interval corresponds to a weather change from almost non-windy environment to a stormy wind condition in approximately 7 minutes, which is not realistic. But still, even though experiencing such a rapid change in sea wave elevations, results of the optimal altitude command generation algorithm are satisfactory. Furthermore, command tracking performance of the Kalman filter based altitude controller does not worsen with changing sea state, it still performs quite adequate.

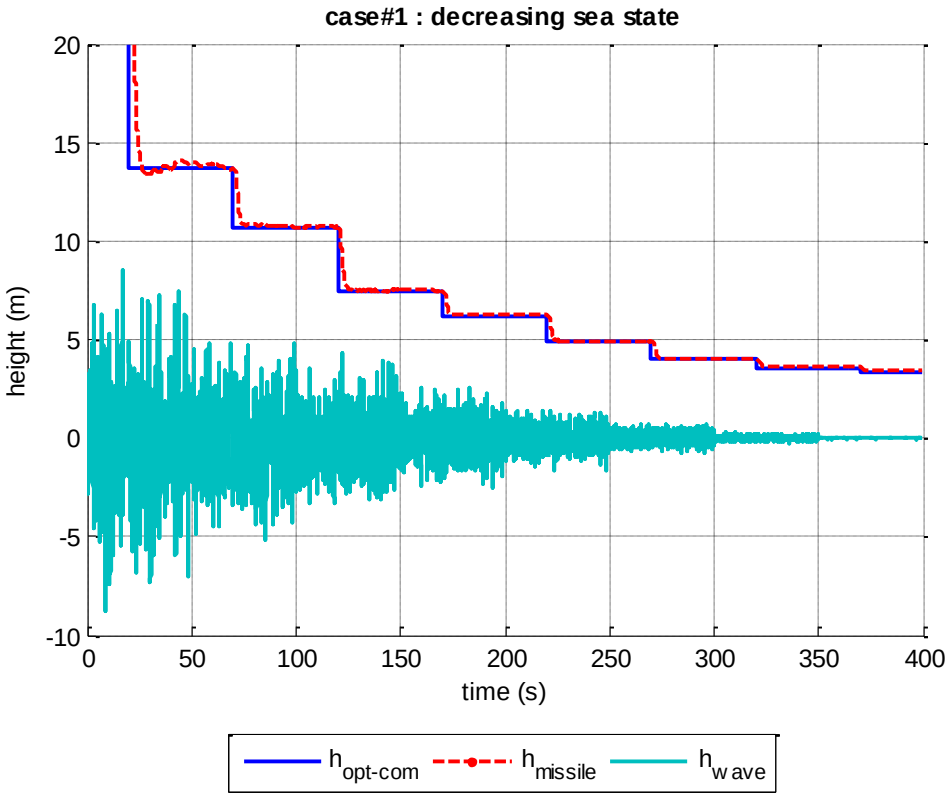

Figure 5.7 : Optimal Altitude Command & Tracking for Decreasing Sea State

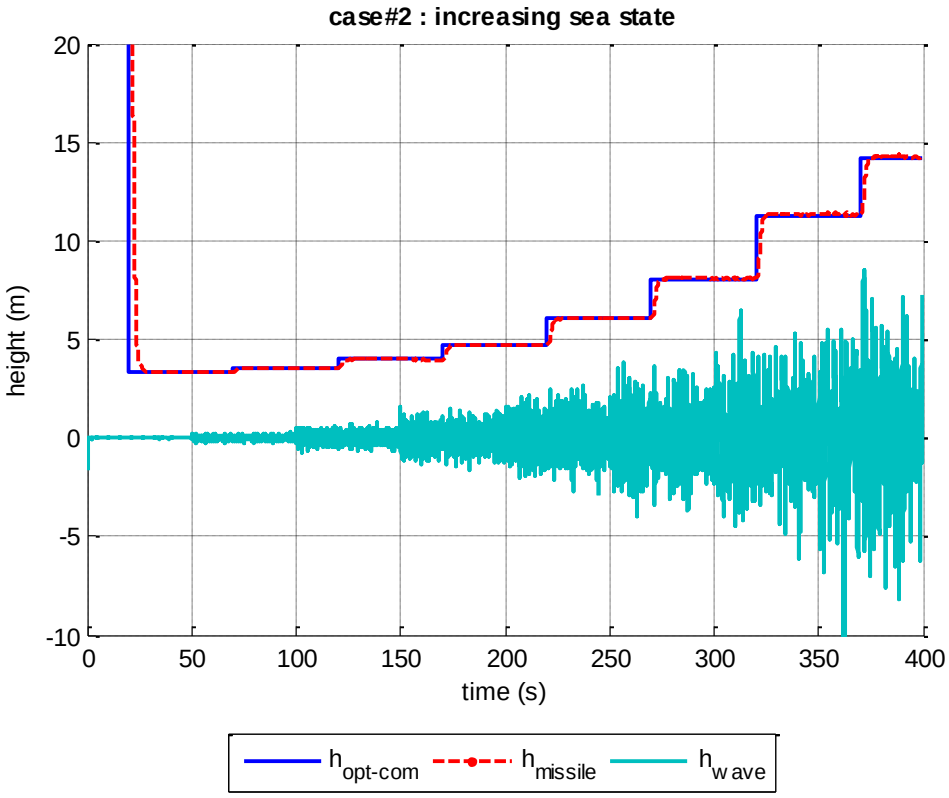

Figure 5.8 : Optimal Altitude Command & Tracking for Increasing Sea State

Note that noise covariance matrix of the Kalman filter is chosen according the worst-case condition. But, one may consider online updating of Kalman filter noise covariance matrix R with the obtained statistics of the wave estimations, as a one more step for a better adaptation to sea condition. By this way, for low sea states estimator trusts altimeter measurements more while for high sea states filter concentrates more on system model rather than noisy measurements. Even though this idea seems very promising in theory, in practice it does not offer a considerable benefit to the system. If this adaptation is applied and compared with the proposed method, the difference in the command tracking performance between worst-case choice and online update of R matrix, does not exceed few centimeters.

CHAPTER 6

CONCLUSION

In this thesis, altitude control considerations of a sea skimming anti-ship missile are addressed. First, altitude control problems due to varying real world effects are analyzed; then, a novel method is presented by means of both determining the optimal flight altitude and smooth tracking of the commanded altitude. Moreover, presented method is compared with the ones already existing in the literature under several test scenarios.

By default, altitude of the missile is controlled by an altitude controller and an acceleration autopilot. Feedbacks of the control system greatly affect the system performance since the default method has no information about the stochastic properties of the measurements. While the unknown accelerometer bias error causes the altitude information in INS to drift, sea wave elevations and radar signal reflections make the RA measurements quite noisy. These phenomena results that, neither pure INS solutions nor direct RA measurements can be used in altitude controller safely. Previous approaches in literature integrate these two-sensor data to obtain a better performance; however, when the problem is approached with whole real world effects all in once, those methods also come up with poor performance.

With a similar idea, yet a different method is developed for the altitude control system design, which is based Kalman filter. KF estimations are performed by utilizing the data from RA and IMU, by considering noisy RA measurements and biased accelerometer measurement as well as with a limited computer. Series of simulation results with different scenarios revealed that, proposed method has a well performance by means of tracking the commanded altitude profile.

Furthermore, by using same KF estimations, instantaneous wave height is acquired, and a method based on statistical nature of sea waves is developed to determine an optimum flight altitude. Commanding this optimum altitude profile to the altitude control guarantees missile to fly as low as it can according to the environmental conditions. All in all, proposed combined method in this study provides robustness to the altitude control system of the missile against many real world issues.

If one needs to perform further analyses about this specific topic, the present study can be investigated and improved with following considerations;

- Missile model can be extended to six degree of freedom nonlinear model; such that, performance of the altitude controller can be analyzed with coupling effects due to roll and yaw plane disturbances. Especially during a maneuver in yaw plane, one may expect the performance of the altitude controller to be disturbed.
- Aerodynamic database uncertainties, which may cause the autopilot performance to be different than expected, can be addressed and overall effect on the altitude control act can be analyzed.
- Although major accelerometer error, which is bias, is considered, other IMU errors such as miss-alignment, scale factor and random walk can be introduced, and the response can be observed.
- Different RA noise levels can be introduced, and the estimation performance can be investigated.
- Different sea wave models with wind blowing varying directions can be introduced and success of the designed controller can be examined.
- Proposed Kalman filter assumes that both process and measurement noises are white; i.e., noise occurs at each frequency component with same magnitude. But in fact, varying sea conditions cause the altimeter measurements to be somewhat colored. For this reason, Kalman filter may be modified to deal with colored measurement noise and results can be studied.

All in all, within the scope of addressed errors and disturbances in this study, a novel method is developed for altitude control system of a sea skimming missile. Having analyzed the results of numerous simulations, it can noticeably be deducted that, proposed control method is very successful in each separate case. As a result, the method presented here provides robustness to the system against many real world issues.

REFERENCES

[1] N. Friedman, The Naval Institute Guide to World Naval Weapons Systems, Naval Institute Press, 1997.

[2] D. R. Ousborne, "Ship Self-Defense Against Air Threads," *John Hopkins APL Technical Digest,* vol. 14, no. 2, pp. 125-140, 1993.

[3] J. C. Schulte, "An Analysis of the Historical Effectiveness of Anti-Ship Cruise Missiles in Littoral Warfare," Naval Postgraduate School, Monterey, 1994.

[4] X. Zhao and X. Fan, "A Method Based on Genetic Algorithm for Anti-Ship Missile Path Planning," in *IEEE International Joint Conference on Computational Sciences and Optimization*, Sanya, 2009.

[5] G. Liu, S. Y. Lao, D. F. Tan and Z. C. Zhou, "Research Status and Progress on Anti-Ship Missile Path Planning," *Acta Automatica Sinica,* vol. 39, no. 4, pp. 347-359, 2013.

[6] C. K. Ryoo, H. S. Shin and M. J. Tahk, "Energy Optimal Waypoint Guidance Synthesis for Antiship Missiles," *IEEE Transactions on Aerospace and Electronical Systems,* vol. 46, no. 1, pp. 80-95, 2010.

[7] B. Jung and Y. Kim, "Guidance Laws for Anti-Ship Missiles Using Impact Angle and Impact Time," in *AIAA Guidance, Navigation and Control Conference*, Keystone, 2006.

[8] P. Bauer and A. Dorobantu, "Optimal Waypoint Guidance, Trajectory Design and Tracking," in *American Control Conference*, Washington, 2013.

[9] Y. H. Kim, C. K. Ryoo and M. J. Tahk, "Guidance Synthesis for Evasive Maneuver of Anti-Ship Missiles Against Closed-In Weapon Systems," *IEEE Transactions on Aerospace and Electronic Systems*, vol. 46, no. 3, pp. 1376-1388, 2010.

[10] W. Ra, I. Whang and J. Ahn, "Robust Horizontal Line-of-Sight Rate Estimator for Sea Skimming Anti-Ship Missile with Two-Axis Gimballed Seeker," *IEE Proceedings - Radar, Sonar and Navigation,* vol. 152, no. 1, pp. 9-15, 2005.

[11] E. Kim, H. Cho and Y. Lee, "Terminal Guidance Algorithms of Missiles Maneuvering in the Vertical Plane," in *AIAA Guidance, Navigation and Control Conference*, San Diego, 1996.

[12] J. R. Dowdle, "An Optimal Guidance Law for Supersonic Sea Skimming," in *AIAA Guidance Navigation and Control Conference*, Snowmass, 1985.

[13] J. R. Dowdle, "Bandwidth Requirements for Sea Skimming Guidance," in *AIAA Guidance Navigation and Control Conference*, Snowmass, 1985.

[14] D. J. Lesieutre, D. Nixon, M. F. E. Dillenius and T. O. Torres, "Analysis of Missiles Flying Low Over Various Sea States," in *Atmospheric Flight Mechanics Conference*, Portland, 1990.

[15] D. J. Lesieutre, P. H. Reisenthel, M. F. E. Dillenius, D. Viazzo and S. C. McIntosh, "Unsteady Simulation of Flexible Missiles Flying Low Over the Sea," in *Aerospace Sciences Meeting and Exhibit*, Reno, 1994.

[16] S. E. Talole and S. B. Phadke, "Height Control System for Sea-Skimming Missile Using Predictive Filter," *Journal of Guidance Control and Dynamics,* vol. 25, no. 5, pp. 989-992, 2002.

[17] K. S. Priyamvada, V. Olikal, S. E. Talole and S. B. Phadke, "Robust Height Control System Design for Sea Skimming Missiles," *Journal of Guidance Control and Dynamics*, vol. 34, no. 6, pp. 1746-1756, 2011.

[18] O. Dulgar, R. B. Gezer and A. T. Kutay, "Extended Kalman Filter Based Robust Altitude Controller for Sea Skimming Missiles," in *AIAA Guidance Navigation and Control Conference*, San Diego, 2016.

[19] S. Axelsson and SAAB-MISSILES, "A Method for the Determination of the Optimum Altitude for a Vehicle Flying Low Over a Sea Surface". European Patent EP0250039B1, 10 February 1993.

[20] A. Eluheshi, M. Matausek and J. Zatkalik, *Modeling of Radar Altimeter as the Main Sensor of a High Performance Height Control of Sea Skimming Missile Flying Just Over a Rough Sea,* MEASUREMENTS 12(14), p. 32.

[21] NATO International Staff, Defence Support Division, *Standardized Wave and Wind Environments for NATO Operational Areas,* Allied Naval Engineering Publication, 1983, pp. F-6.

[22] W. J. Pierson, G. Neumann and R. W. James, "Practical Methods for Observing and Forecasting Ocean Waves by means of Wave Spectra and Statistics," U.S. Naval Oceanographic Office, NSTL Station, 1972.

[23] O. M. Faltinsen, Sea Loads on Ships and Offshore Structures, Cambridge: Cambridge University Press, 1990.

[24] W. J. Pierson and L. Moskowitz, "A Proposed Spectral Form for Fully Developed Wind Seas Based on the Similarity Theory of S. A. Kitaigorodskii," New York University School of Engineering and Science Research Division, New York, 1963.

[25] T. I. Fossen, Guidance and Control of Ocean Vehicles, Chichester: John Wiley & Sons Ltd, 1994.

[26] T. Avcıoglu, "A Tool for Trajectory Planning and Performance Verification of Cruise Missiles," M.Sc. Thesis, Middle East Technical University, Ankara, 2000.

[27] Q. Wen, Q. Xia and C. Cai, "Analysis for Height Control Loop of Cruise Missile to Dİfferent Kinds of Autopilot," *Advances in Automation and Robotics,* vol. 2, no. 123, pp. 507-514, 2011.

[28] A. Kahvecioglu, "A Tool for Designing Robust Autopilots for Ramjet Missiles," M.Sc. Thesis, Middle East Technical University, Ankara, 2006.

[29] K. Ogata, Modern Control Engineering, 5th ed., New Jersey: Pearson Prentice Hall, 2010.

[30] J. Kautsky, N. K. Nichols and P. V. Dooren, "Robust Pole Assignment in Linear State Feedback," *International Journal of Control,* vol. 41, no. 5, pp. 1129-1155, 1985.

[31] K. Ogata, System Dynamics, 4th ed., New Jersey: Pearson Prentice Hall, 2004.

[32] C. L. Kirby and R. Hall, "Description and Accuracy Evaluation of the Honeywell Radar Altimeter," Canadian Forestry Service Northern Forest Research Centre, Edmonton, 1980.

[33] P. D. Groves, Principles of GNSS, Inertial and Multisensor Integrated Navigation Systems, Boston: Artech House, 2008.

[34] Honeywell International Inc, "Honeywell Aerospace," [Online]. Available: https://aerospace.honeywell.com/en/products/navigation-and-sensors/hg1700. [Accessed 26 11 2017].

[35] D. Simon, Optimal State Estimation, New Jersey: John Wiley & Sons Inc, 2006.

[36] K. Ogata, Discrete Control Systems, New Jersey: Prentice-Hall, 1995.

[37] J. L. Crassidis and J. L. Junkins, Optimal Estimation of Dynamic Systems, Boca Raton: CRC Press, 2012.

[38] National Institute of Standards and Technology, "NIST Handbook of Mathematical Functions," Cambridge University Press, New York, 2010.

APPENDIX A

DERIVATION OF EQUATIONS OF MOTION

Equations of motion consist of three force and three moment equations which can be derived from translational and rotational dynamics of the air vehicle.

Translational Dynamics

Total force is defined as the time derivative of the linear momentum with respect to the inertial frame;

$$\vec{F} = D_0\left(\vec{L}\right) \qquad ; \qquad \vec{L} = m\vec{V} \tag{A.1}$$

Considering the force and velocity vector is meaningful in body fixed axis of the vehicle, writing the equations in body fixed frame;

$$\begin{aligned} \bar{F}^{(b)} &= D_b\left(m\bar{V}^{(b)}\right) + \bar{\omega}_{b/0}^{(b)} \times \left(m\bar{V}^{(b)}\right) \\ \bar{F}^{(b)} &= \dot{m}\bar{V}^{(b)} + m\dot{\bar{V}}^{(b)} + \bar{\omega}_{b/0}^{(b)} \times (m\bar{V}^{(b)}) \end{aligned} \tag{A.2}$$

Assuming mass is constant with time and writing the equations in column matrix form yields;

$$\begin{bmatrix} F_x \\ F_y \\ F_z \end{bmatrix} \frac{1}{m} = \begin{bmatrix} \dot{u} \\ \dot{v} \\ \dot{w} \end{bmatrix} + \begin{bmatrix} p \\ q \\ r \end{bmatrix} \times \begin{bmatrix} u \\ v \\ w \end{bmatrix} \tag{A.3}$$

Separating the equations;

$$\begin{aligned} F_x/m &= \dot{u} + qw - rv \\ F_y/m &= \dot{v} + ru - pw \\ F_z/m &= \dot{w} + pv - qu \end{aligned} \tag{A.4}$$

Rotational Dynamics

Total moment is defined as the time derivative of the angular momentum;

$$\Sigma\vec{M} = \frac{d(\vec{H})}{dt} \qquad ; \qquad \vec{H} = \hat{J}\vec{\omega} \tag{A.5}$$

Considering the moment and angular velocity vector is meaningful in body fixed axis of the vehicle, writing the equations in body fixed frame;

$$\begin{aligned} \bar{M}^{(b)} &= D_b\left(\hat{J}^{(b)}\bar{\omega}_{b/0}^{(b)}\right) + \bar{\omega}_{b/0}^{(b)} \times \left(\hat{J}^{(b)}\bar{\omega}_{b/0}^{(b)}\right) \\ \bar{M}^{(b)} &= \dot{\hat{J}}^{(b)}\bar{\omega}_{b/0}^{(b)} + \hat{J}^{(b)}\dot{\bar{\omega}}_{b/0}^{(b)} + \bar{\omega}_{b/0}^{(b)} \times (\hat{J}^{(b)}\bar{\omega}_{b/0}^{(b)}) \end{aligned} \tag{A.6}$$

Assuming inertia is constant with time in body fixed frame and writing the equations in column matrix form yields;

$$\begin{bmatrix} M_x \\ M_y \\ M_z \end{bmatrix} = \begin{bmatrix} I_{xx} & I_{xy} & I_{xz} \\ I_{yx} & I_{yy} & I_{yz} \\ I_{zx} & I_{zy} & I_{zz} \end{bmatrix} \begin{bmatrix} \dot{p} \\ \dot{q} \\ \dot{r} \end{bmatrix} + \begin{bmatrix} p \\ q \\ r \end{bmatrix} \times \left(\begin{bmatrix} I_{xx} & I_{xy} & I_{xz} \\ I_{yx} & I_{yy} & I_{yz} \\ I_{zx} & I_{zy} & I_{zz} \end{bmatrix} \begin{bmatrix} p \\ q \\ r \end{bmatrix} \right) \tag{A.7}$$

Separating the equations;

$$\begin{aligned} M_x &= I_{xx}\dot{p} - I_{yz}(q^2 - r^2) - I_{zx}(\dot{r} + pq) - I_{xy}(\dot{q} - rp) - \left(I_{yy} - I_{zz}\right)qr \\ M_y &= I_{yy}\dot{q} - I_{zx}(r^2 - p^2) - I_{xy}(\dot{p} + qr) - I_{yz}(\dot{r} - pq) - (I_{zz} - I_{xx})rp \\ M_z &= I_{zz}\dot{r} - I_{xy}(p^2 - q^2) - I_{yz}(\dot{q} + rp) - I_{zx}(\dot{p} - qr) - \left(I_{xx} - I_{yy}\right)pq \end{aligned} \tag{A.8}$$

In the equations above, $F_x, F_y, F_z, M_x, M_y, M_z$ are the resulting aerodynamic, propulsive and gravitational forces and moments acting on the missile, in body fixed frame.

Euler Angle Rates and Body Rates

Just for the sake of completeness, relation between Euler rates and body angular rates can be derived from kinematic equations which involve the transformation matrices by 3-2-1 Euler sequence of rotations;

$$\begin{bmatrix} p \\ q \\ r \end{bmatrix} = \hat{T}_1(\phi)\begin{bmatrix} \dot{\phi} \\ 0 \\ 0 \end{bmatrix} + \hat{T}_1(\phi)\hat{T}_2(\theta)\begin{bmatrix} 0 \\ \dot{\theta} \\ 0 \end{bmatrix} + \hat{T}_1(\phi)\hat{T}_2(\theta)\hat{T}_3(\psi)\begin{bmatrix} 0 \\ 0 \\ \dot{\psi} \end{bmatrix} \tag{A.9}$$

Where transformation matrices in open form are as follows;

$$\hat{T}_1(\phi) = \begin{bmatrix} 1 & 0 & 0 \\ 0 & cos\phi & sin\phi \\ 0 & -sin\phi & cos\phi \end{bmatrix}$$
$$\hat{T}_2(\theta) = \begin{bmatrix} cos\theta & 0 & -sin\theta \\ 0 & 1 & 0 \\ sin\theta & 0 & cos\theta \end{bmatrix} \quad \text{(A.10)}$$
$$\hat{T}_3(\psi) = \begin{bmatrix} cos\psi & sin\psi & 0 \\ -sin\psi & cos\psi & 0 \\ 0 & 0 & 1 \end{bmatrix}$$

Then, the kinematic relation becomes;

$$\dot{\phi} = p + qsin\theta tan\theta + rcos\phi tan\theta$$
$$\dot{\theta} = qcos\phi - rsin\phi \quad \text{(A.11)}$$
$$\dot{\phi} = (qsin\phi + rcos\phi)sec\theta$$

APPENDIX B

LINEARIZATION OF EQUATIONS OF MOTION FOR PITCH PLANE

For a sea skimming cruise missile, which is the subject of this study, following assumptions can be made;

- X-Z plane of the body fixed coordinate system of the missile is a plane of symmetry. Moreover, principal axes are located at center of gravity of the missile and assuming this is a cruciform missile;

$$I_{xy} = I_{yz} = I_{xz} = 0 \tag{B.1}$$

- Roll angle and roll rate are already compensated by a roll autopilot in a much faster fashion compared to pitch autopilot. Furthermore, since the focus is on the pitch plane, there is no motion in yaw plane;

$$\begin{aligned} \dot{p} = p = \phi = 0 \\ \dot{r} = r = 0 \end{aligned} \tag{B.2}$$

- Missile is flying with a constant speed within a small angle of attack interval;

$$\begin{aligned} u \approx V = constant \\ \alpha = \tan^{-1}\frac{w}{u} \approx \frac{w}{u} \\ \dot{\alpha} \approx \frac{\dot{w}}{u} \approx \frac{\dot{w}}{V} \end{aligned} \tag{B.3}$$

Applying these assumptions to the related equations of motion derived in APPENDIX A, following equations are obtained.

Third equation of (A.4) simplifies to;

$$\dot{w} = \frac{F_z}{m} + qu = a_z + qu \tag{B.4}$$

Second equation of (A.8) simplifies to;

$$\dot{q} = \frac{M_y}{I_{yy}} \tag{B.5}$$

Second equation of (A.11) simplifies to;

$$\dot{\theta} = q \tag{B.6}$$

Substituting (B.4) into third equation of (B.3) and directly writing (B.5) yields following two equations.

$$\begin{aligned} \dot{\alpha} &= \frac{F_z/m + qu}{u} = \frac{F_z}{mu} + q \approx \frac{F_z}{mV} + q \\ \dot{q} &= \frac{M_y}{I_{yy}} \end{aligned} \tag{B.7}$$

The resulting force and moment acting on the missile involves aerodynamic and gravitational components;

$$\begin{aligned} F_z &= QS_{ref}c_z + mg_z \\ M_y &= QS_{ref}l_{ref}c_m \end{aligned} \tag{B.8}$$

Here, non-dimensional aerodynamic coefficients c_z and c_m are calculated through Taylor series expansion with aerodynamic stability derivatives. Moreover, gravitational component is calculated through trigonometric relationship.

$$\begin{aligned} c_z &= c_{z_\alpha}\alpha + c_{z_q}q + c_{z_\delta}\delta \\ c_m &= c_{m_\alpha}\alpha + c_{m_q}q + c_{m_\delta}\delta \\ g_z &= g\cos\theta \end{aligned} \tag{B.9}$$

One can define the dimensional aerodynamic derivatives as follows;

$$
\begin{aligned}
Z_\alpha &= c_{z_\alpha} * \frac{QS_{ref}}{m} & M_\alpha &= c_{m_\alpha} * \frac{QS_{ref} l_{ref}}{I_{yy}} \\
Z_q &= c_{z_q} * \frac{QS_{ref}}{m} \frac{l_{ref}}{2V} & M_q &= c_{m_q} * \frac{QS_{ref}}{I_{yy}} \frac{l_{ref}^2}{2V} \\
Z_\delta &= c_{z_\delta} * \frac{QS_{ref}}{m} & M_\delta &= c_{m_\delta} * \frac{QS_{ref} l_{ref}}{I_{yy}}
\end{aligned}
\tag{B.10}
$$

Combining the equations (B.7) to (B.10) returns the following linear model.

$$
\begin{aligned}
\begin{bmatrix} \dot{\alpha} \\ \dot{q} \end{bmatrix} &= \begin{bmatrix} \frac{Z_\alpha}{V} & \frac{Z_q}{V} + 1 \\ M_\alpha & M_q \end{bmatrix} \begin{bmatrix} \alpha \\ q \end{bmatrix} + \begin{bmatrix} \frac{Z_\delta}{V} & \frac{1}{V} \\ M_\delta & 0 \end{bmatrix} \begin{bmatrix} \delta \\ g_z \end{bmatrix} \\
a_z &= \begin{bmatrix} Z_\alpha & Z_q \end{bmatrix} \begin{bmatrix} \alpha \\ q \end{bmatrix} + \begin{bmatrix} Z_\delta & 1 \end{bmatrix} \begin{bmatrix} \delta \\ g_z \end{bmatrix}
\end{aligned}
\tag{B.11}
$$

APPENDIX C

DEFINITION OF THE ERROR FUNCTION

The error function, also called the Gaussian error function, is a non-elementary mathematical function. It is of sigmoid shape and occurs in probability, statistics and some partial differential equations. Error function is defined in equation (C.1) [38].

$$\text{erf}(z) = \frac{2}{\sqrt{\pi}} \int_0^z e^{-t^2}\ dt \tag{C.1}$$

Complementary error function is defined as in (C.2).

$$\text{erfc}(x) = \frac{2}{\sqrt{\pi}} \int_z^\infty e^{-t^2}\ dt = 1 - \text{erf}(z) \tag{C.2}$$

Error function does not have an analytical solution, but it can be solved by several numerical methods depending on the problem. Most frequently used method is the power series expansion given in (C.3).

$$\text{erf}(z) = \frac{2}{\sqrt{\pi}} \sum_{n=0}^{n=\infty} \frac{(-1)^n\, z^{2n+1}}{n!\,(2n+1)} \tag{C.3}$$

Inverse of the error function is defined as in (C.4). By definition, error function of the inverse error function of a variable is itself, while the variable is bounded within ± 1 interval. Note that, equation in (C.1) is already bounded within ± 1.

$$\begin{gathered} y = \text{erf}(x) \quad \rightarrow \quad x = \text{erf}^{-1}(y) \\ \text{erf}(\text{erf}^{-1}(z)) = z \quad ; \quad -1 \leq z \leq 1 \end{gathered} \tag{C.4}$$

Series expansion of the inverse error function is as in equation (C.5).

$$\operatorname{erf}^{-1}(z) = \sum_{k=0}^{\infty} \frac{c_k}{2k+1} \left(\frac{\sqrt{\pi}}{2} z \right)^{2k+1}$$
$$c_0 = 1 \quad ; \quad c_k = \sum_{m=0}^{k-1} \frac{c_m c_{k-1-m}}{(m+1)(2m+1)} \tag{C.5}$$